Magnesium modulates phospholipid metabolism to promote bacterial phenotypic resistance to antibiotics

Hui Li[1,2,†], Jun Yang[1,2,†], Su-fang Kuang[1], Bo Peng[1,2,*]

[1]*State Key Laboratory of Bio-Control, School of Life Sciences, Southern Marine Science and Engineering Guangdong Laboratory (Zhuhai), Guangdong Province Key Laboratory for Pharmaceutical Functional Genes, Sun Yat-sen University, Higher Education Mega Center, Guangzhou 510006, People's Republic of China.*

[2] *Laboratory for Marine Biology and Biotechnology, Marine Fisheries Science and Food Production Processes, Qingdao National Laboratory for Marine Science and Technology, Qingdao 266071, China.*

[†] These authors contributed equally to this work

Running title: magnesium induces bacterial phenotypic resistance

[*]**Corresponding author:** Bo Peng (email: pengb26@mail.sysu.edu.cn) *State Key Laboratory of Bio-Control, School of Life Sciences, Sun Yat-sen University, Guangzhou 510275, People's Republic of China*.

Abstract

Non-inheritable antibiotic resistance or phenotypic resistance ensures bacterial survival upon antibiotic treatment. However, exogenous factors in promoting phenotypic resistance is poorly defined. Here, we demonstrate that *Vibrio alginolyticus* are recalcitrant to killing by a broad spectrum of antibiotics under high magnesium. Functional metabolomics demonstrate that magnetism modulates the biosynthesis of fatty acids in increasing the biosynthesis of saturated fatty acids while decreasing unsaturated fatty acids. Exogenous supplementation of fatty acids confirm the role of fatty acids in antibiotic resistance. Furthermore, functional lipidomics reveal that glycerophospholipid metabolism is the major metabolic pathway remodeled by magnetism, where the biosynthesis of PE is decreased but PG is increased. Thus, the membrane composition is altered, leading to increased membrane polarization, and decreased permeability and fluidity. These together reduce the uptake of antibiotics by the bacteria. Thus, our study suggest a previously unrecognized metabolic mechanism by which bacteria escape antibiotic killing by utilizing environmental factor.

Keywords:

magnesium, phenotypic resistance, quinolones, phospholipid metabolism, membrane fluidity

Introduction

Non-inheritable antibiotic resistance or phenotypic resistance represent a serious therapeutic challenge for bacterial infectious diseases. Phenotypic resistance does not involve genetic mutations, instead, this type of resistance are transient. Thus, bacteria resume to normal growth after removing the antibiotics. Two extensively studied phenotypic resistance includes biofilm and bacterial persisters (Corona & Martinez, 2013). Biofilms have complex structures that impede the diffusion of antibiotics and contain elements sequestrating antibiotics to prevent their further actions (Ciofu *et al*, 2022). Moreover, biofilm-forming bacteria and persisters themselves have distinct metabolic state that also significantly negatively influence their susceptibility to antibiotics (Yan & Bassler, 2019). These two types of phenotypic resistance have common phenomena that their growth are retarded or even stopped in the presence of antibiotics (Corona & Martinez, 2013). However, factors promoting bacterial phenotypic resistance that is still proliferate in the presence of antibiotics are poorly defined.

There is a growing body of evidence that metal ions have diverse impact on chemical, physical and physiological phenomena that play roles in development of antibiotic resistance (Booth *et al*, 2011; Lu *et al*, 2020; Poole, 2017). One mechanism could involve genetic elements that harbor genes conferring resistance to metals and antibiotics (Poole, 2017) . On the other hand, recent reports suggest that metal cations directly hinder (or enhance) the activity of specific antibiotic drugs (Zhang *et al*, 2014) and that the metabolic environment impacts bacterial sensitivity to antibiotics (Jiang *et*

al, 2023; Lee & Collins, 2012; Peng *et al*, 2015; Zhang *et al*, 2020; Zhao *et al*, 2021). Light metal ions, such as magnesium, sodium, and potassium, serve as cofactors to many enzymes (Du *et al*, 2016), some of which could influence drug efficacy. Heavy metal ions, including Cu^{2+} and Zn^{2+}, confer resistance to antibiotics (Yazdankhah *et al*, 2014; Zhang *et al*, 2018). Recent reports suggest that sodium negatively regulates redox states to promote antibiotic resistance in *Vibrio alginolyticus* (Yang *et al*, 2018), while actively growing *Bacillus subtilis* cope with ribosome-targeting antibiotics based on ion flux modulation (Lee *et al*, 2019). But whether such ions can promote phenotypic resistance is less explored.

Results

Mg^{2+} promotes resistance to antibiotics

Magnesium is rich in marine and marine aquaculture, where antibiotics are commonly used. We directly investigate the effect of Mg^{2+} on balofloxacin (BLFX) susceptibility in two strains of *Vibrios*, *V. alginolyticus* ATCC33787 and *V. parahaemolyticus* VP01, which were isolated from marine aquaculture. In the initial experiment, the ionic environment of marine water was simulated by adding 39 mM NaCl, 35 mM Mg_2SO_4, 7 mM KCl, and 7 mM $CaCl_2$ to LB medium (**Table EV1**), to create a medium which we designated "artificial seawater" (ASWT). The minimum inhibitory concentrations (MIC) for BLFX in ATCC33787 and VP01 were 54 μg/mL and 25 μg/mL in ASWT and 1 μg/mL and 3 μg/mL in LB medium, respectively (**Fig 1A**). The role of exogenous NaCl in antibiotic resistance was investigated in a previous study (Yang *et al.*, 2018);

and the MIC for BLFX was the same in LB medium or M9 medium plus 7 mM KCl or 7 mM $CaCl_2$ (**Fig EV1**). However, the MIC for BLFX was higher in M9 medium plus Mg_2SO_4 or $MgCl_2$ (**Fig 1B**) and the MIC for BLFX increased with increasing concentration of $MgCl_2$. Specifically, addition of 50 mM or 200 mM $MgCl_2$ increased the MIC for BLFX 200- or 1600-fold, respectively (**Fig 1B**). Using the Oxford cup method, the zone of inhibition increased with increasing $MgCl_2$ from 15.6 mM – 62.4 mM (**Fig 1D**). Exogenous $MgCl_2$ also increased MICs for other quinolones (*e.g.* nalidixic acid, levofloxacin, ciprofloxacin, ofloxacin, and moxifloxacin (**Fig 1E**) and non-quinolone antibiotics including antibacterial peptides (colistin), macrolides (roxithromycin), tetracyclines (oxytetraycline), β-lactams (ceftriaxone, ceftazidime), and aminoglycosides (amikacine, kanamycin, and gentamicin) (**Fig 1F**). Such non-specific resistance promoting effects indicate that Mg^{2+} promotes phenotypic resistance.

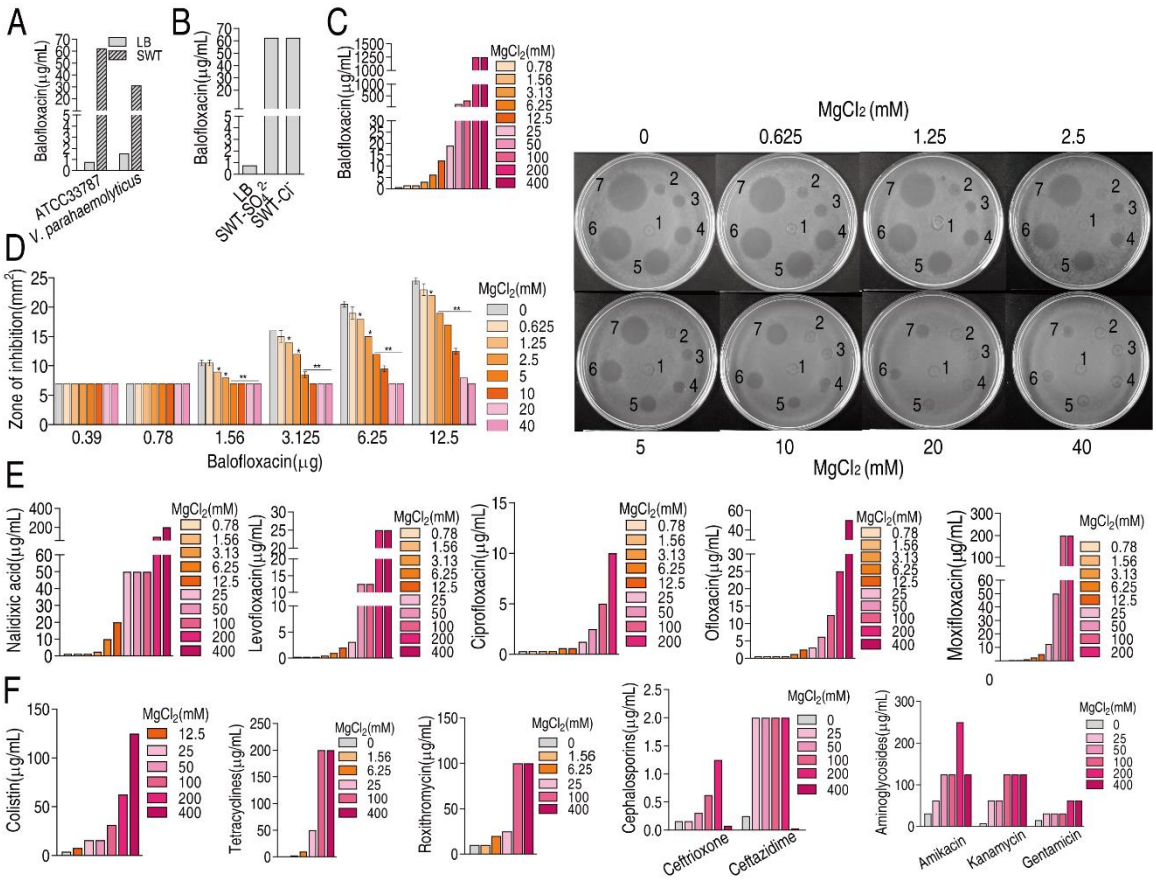

Figure 1. Magnesium promotes bacterial resistance to antibiotics. A. MIC of ATCC 33787 and *V. parahaemolyticus* to BLFX in SWT or LB medium by microtitre-dilution-method. **B.** MIC of ATCC 33787 to BLFX in SWT with the replacement of $MgCl_2$ with $MgSO_4$ $MgCl_2$ by microtitre-dilution-method. **C.** MIC of ATCC 33787 to BLFX in SWT with the indicated concentrations of $MgCl_2$ by microtitre-dilution-method. **D.** MIC of ATCC 33787 to BLFX in the indicated concentrations of BLFX and $MgCl_2$ by Oxford cup test. **E.** MIC of ATCC 33787 to other quinolones in SWT with the indicated concentrations of $MgCl_2$ by microtitre-dilution-method. **F.** MIC of ATCC 33787 to other classes of antibiotics in SWT with the indicated concentrations of $MgCl_2$ by microtitre-dilution-method.

Extracellular Mg^{2+}, intracellular Mg^{2+} and chelation of antibiotic

Previous reports suggest that chelation of antibiotics by magnesium ions inhibits antibiotic uptake (Deitchman *et al*, 2018; Lunestad & Goksøyr, 1990). To explore this

possibility, the zone of inhibition for balofloxacin was measured with various concentrations of $MgCl_2$, ranging from 0 mM to 200 mM. Marine water usually contains 50 mM $MgCl_2$. Lower concentrations of $MgCl_2$, (0.78, 3.125 or 12.5 mM) did not alter the zone of inhibition, while higher concentration including 50 and 200 mM $MgCl_2$ decreased the zone of inhibition (**Fig 2A**). Correlation of the $MgCl_2$ concentration-dependent resistance suggests that chelation influences bacterial survival by 25.5% and 27.7% in 50 and 200 mM $MgCl_2$, respectively, but not at lower $MgCl_2$ concentrations (**Fig 2B & 2C**). Furthermore, intracellular balofloxacin decreased with increasing concentration of $MgCl_2$ (**Fig 2D**), while exogenous Mg^{2+} increased intracellular Mg^{2+} level in a dose-dependent manner, where 50 and 200 mM $MgCl_2$ increased 1.21 and 1.31 mmol/L, respectively (**Fig 2E**). We also examined rate of efflux and expression of LPS, which contribute to antibiotic resistance (Kobylka *et al*, 2020; Song *et al*, 2020). The results show that expression of TolC/*tolC* and LPS was unaffected by Mg^{2+} (**Fig 2F** and **2G**). Loss of *waaF*, *lpxA*, and *lpxC*, three key genes involved in LPS biosynthesis, did not influence sensitivity/resistance to balofloxacin (**Fig 2H**). These data demonstrate that influx of Mg^{2+} plays roles in balofloxacin resistance.

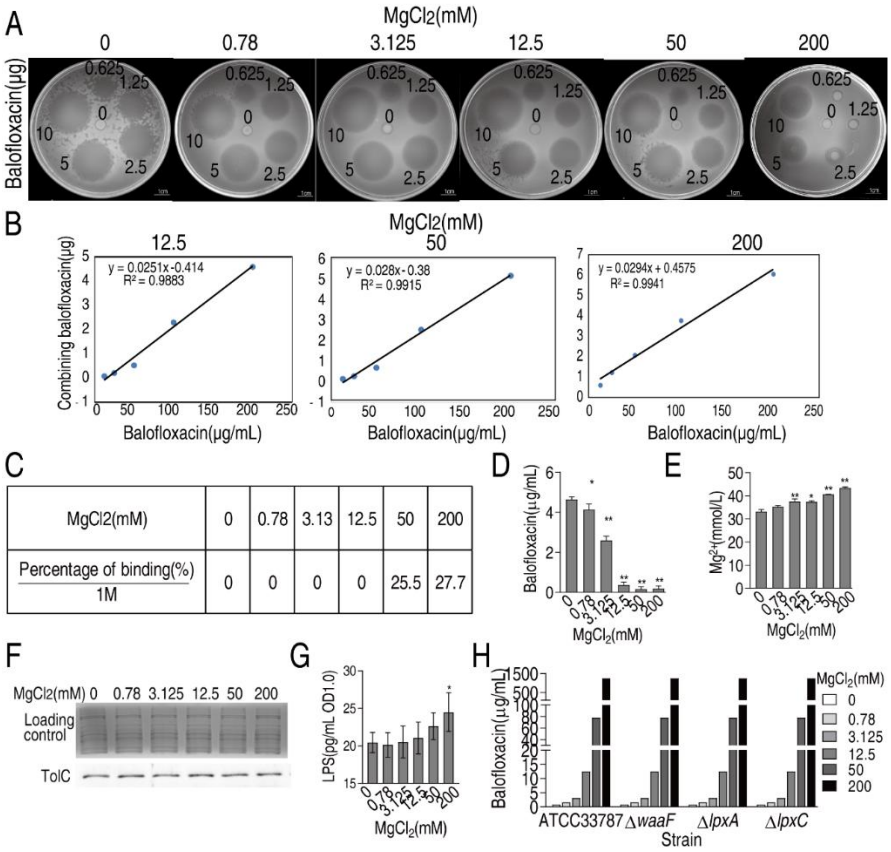

Figure 2. Mg^{2+} elevates intracellular Mg^{2+} and promotes balofloxacin uptake. A. Oxford cup test of 0, 12.5, 25, 50, 100, 200 μg/mL BLFX to ATCC33787 following by separately incubation with the indicated concentrations of $MgCl_2$ for 5 h. **B.** Inhibitory curve of data **(A)**. **C.** Binding efficacy of **(A)**. **D.** Intracellular BLFX of ATCC 33787 in SWT with the indicated concentrations of $MgCl_2$ and 60 μg/mL BLFX. **E.** Intracellular Mg^{2+} of ATCC 33787 in SWT with the indicated concentrations of $MgCl_2$. **F.** Western blot for abundance of TolC in the presence of $MgCl_2$. **G.** LPS quantification at indicated concentrations of $MgCl_2$. **H.** MIC of ATCC 33787 and its mutants Δ*waaF*、Δ*lpxA*、Δ*lpxC* in SWT with the indicated concentrations of $MgCl_2$, which is measured by microtitre-dilution-method.

$MgCl_2$ affects bacterial metabolism

Although it is well established that Mg^{2+} regulates the activity of many metabolic enzymes and strongly influences bacterial metabolism(Garfinkel & Garfinkel, 1985),

the mechanism of Mg^{2+} in promoting antibiotic resistance is less explored. Thus, *V. alginolyticus* was cultured in M9 medium in the presence of various amounts of $MgCl_2$ (0 mM, 0.78 mM, 3.125 mM, 12.5 mM, 50 mM, or 200 mM), analyzed by GC-MS, and identified 54 metabolites. Five biological and two technical replicates were included for each treatment (**Fig EV2**). Rank-sum test and a permutation test were used to identify differentially expressed metabolites. Forty-one metabolites were identified ($p < 0.05$) (**Fig 3A**), which were presented as a heatmap and Z-value in **Fig EV3**. Orthogonal partial least square discriminant analysis (OPLS-DA) was conducted that separated the six treatments into three groups: Group 1 included 0 mM, 0.78 mM, and 3.125 mM $MgCl_2$; Group 2 was a singlet of 12.5 mM; Group 3 included 50 mM and 200 mM $MgCl_2$. Component t[1] distinguishes Group 1 from Groups 2 and 3; component t[2] distinguishes Group 3 from Groups 1 and 2 (**Fig 3B**). Discriminating variables are shown as S-plot, where cut-off values are ≥ 0.05 absolute value of covariance p and 0.5 for correlation p(corr). Six biomarkers/metabolites were selected from component t[1] and p[1]. More specifically, the abundance of cadaverine, urea, palmitic acid, aminoethanol, and fumaric acid were increased, but pyroglutamic acid and glutamic acid were decreased (**Fig 3C; Fig EV4**). Pathway enrichment analysis suggests that twelve pathways are involved. Notably, one of the pathways is biosynthesis of unsaturated fatty acids (terminology in the software. Actually, it is biosynthesis of fatty acids) (**Fig 3D**). Interestingly, the abundance of palmitic acid and stearic acid were increased in an Mg^{2+} dose-dependent manner (**Fig 3E; Fig EV5**). Moreover, palmitic acid was a crucial biomarker (**Fig 3C**). Exogenous palmitic acid

increased bacterial resistance to balofloxacin (**Fig 3F**). These results suggest that fatty acid metabolism may be critical to the resistance.

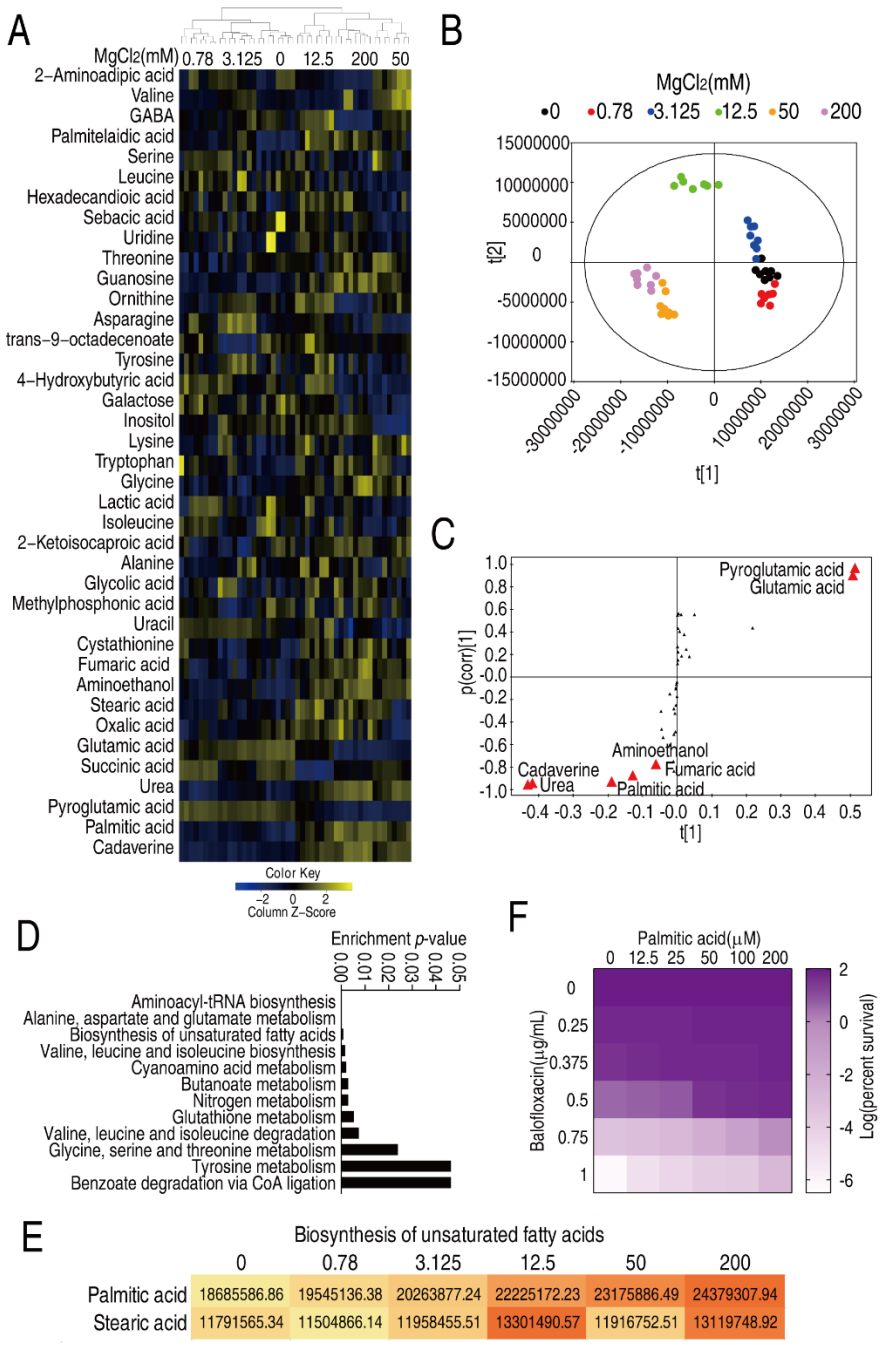

Figure 3. Mg^{2+}-induced metabolomics. A. Differential metabolomes in the absence or presence of the indicated concentrations of $MgCl_2$. Yellow color and blue color indicate increase and decrease of metabolites relative to the median metabolite level, respectively (see color scale). **B.** PCA analysis of different concentrations of $MgCl_2$-

induced metabolomes. Each dot represents the technical replicate of samples in the plot. **C.** S-plot generated from OPLS-DA. Predictive component p [1] and correlation p(corr) [1] differentiate 0, 0.78, 3.125 mM $MgCl_2$ from 12.5, 50, 200 mM $MgCl_2$. Predictive component p[2] and correlation p(corr)[2] separate 0, 0.78, 50, 200 mM $MgCl_2$ from 3.125, 12.5 mM $MgCl_2$. The triangle represents metabolites in which candidate biomarkers are marked. **D.** Enriched pathways by differential abundances of metabolites. **E.** Scatter plot of palmitic acid and stearic acid in the indicated concentrations of $MgCl_2$, which comes from data (**A**). **F.** Synergy analysis for alofloxacin with palmitic acid for *V. algilyticus*. Synergy is represented using a color scale or an isobologram, which compares the dose needed for 50% inhibition for synergistic agents (white) and non-synergistic (i.e., additive) agents (purple).

Mg^{2+} regulates fatty acid biosynthesis

Fatty acids include saturated and unsaturated fatty acids whose biosynthesis shared common biosynthetic pathways from acetyl-CoA to enoyl-ACP, sequentially mediated by *fabD* or *fabH*, *fabB*/*F*, *fabG* and *fabA*/*Z*. Enoyl-ACP is the direct source to produce unsaturated fatty acids or is metabolized to Acyl-ACP via *fabV* to produce saturated fatty acids. Unsaturated fatty acids produce saturated fatty acids via *tesA*/*B* and *yciF*. qRT-PCR was used to quantify the expression of involved genes in bacteria treated with different concentration of $MgCl_2$. The expression of 18 genes was increased when treated with 50 or 200 mM $MgCl_2$ (**Fig 4A**). The increased expression of FabF was confirmed by Western blot (**Fig 4B**). Expression of *tesA*, *tesB*, and *yciA*, which convert unsaturated to saturated fatty acids, was increased (**Fig 4C**). The expression of *fabA* that promotes enoyl-ACP and biosynthesis of unsaturated fatty acids was decreased (**Fig 4D**), which was confirmed at protein level with Western blot (**Fig 4B)**. Oxazole-

2-amine and triclosan inhibit synthesis of fatty acids and decrease bacterial survival in the presence of balofloxacin (**Fig 4E**). These results indicate that Mg^{2+} inhibits synthesis of unsaturated fatty acids and promotes synthesis of saturated fatty acids.

We also quantified the gene expression of fatty acid degradation (**Fig 4F**). Interestingly, the expression of genes involved in unsaturated fatty acid degradation was decreased in an $MgCl_2$ dose-dependent manner (**Fig 4G**), while the expression of genes for exogenous fatty acid degradation was increased. Western blot data confirmed that the abundance of FadL decreased with increasing $MgCl_2$ (**Fig 4H**). FadH degrades unsaturated fatty acids, and influences the ratio of unsaturated to saturated fatty acids. In general, these results suggest that $MgCl_2$ inhibits degradation of fatty acids.

FabR, FadR, ArcA, and cAMP/CRP are transcriptional factors in regulating fatty acid biosynthesis. FabR inhibits biosynthesis of unsaturated fatty acids; FadR promotes biosynthesis and inhibits fatty acids degradation; ArcA and cAMP/CRP inhibit and promote fatty acid degradation, respectively (Feng & Cronan, 2010; Fujita *et al*, 2007). The expression of *fabR* and *fadR* was increased, *arcA* was decreased. The expression of N646_1004 did not change with increasing $MgCl_2$, while expression of N646_1885 increased only in the presence of 200 mM $MgCl_2$ (**Fig 4I**). Western blot data confirmed the decreased expression of FadR with increasing $MgCl_2$ concentration (**Fig 4J**). Viability of Δ*fadR* and Δ*arcA* was decreased in the presence of $MgCl_2$, balofloxacin or both in a dose-dependent manner (**Fig 4K**). Thus, FadR and ArcA could play roles in

bacterial resistance to balofloxacin, presumably by a mechanism that is linked to the abundance of saturated/unsaturated fatty acids.

Furthermore, to investigate whether Mg^{2+} functions through FadR and ArcA, expression of 8 genes of fatty acid biosynthetic genes (*accA*, *accC*, *fabD*, *fabH*, *fabR*, *fabG*, *fabV*, and *yciA*) and 5 genes of fatty acid degradation (*fadL*, *fadD*, *fadB*, and *fadA*) were quantified in wildtype, Δ*fadR* and Δ*arcA* bacterial strains. As expected, the expression of fatty acid biosynthetic genes was decreased in Δ*fadR* cells (**Fig 4L**). However, higher expression of *fadD*, *fadB*, and *fadA* (elevated *fadA* only for Δ*fadR*) was detected in Δ*fadR* or ΔacrA strains, but the expression of these genes was negatively regulated by 200 mM $MgCl_2$ (**Fig 4M-O**). These results indicate that Mg^{2+} promotes biosynthesis of fatty acids by positively regulating *fadR*, and inhibits degradation of fatty acids through *fadR*, *arcA* and their downstream targets.

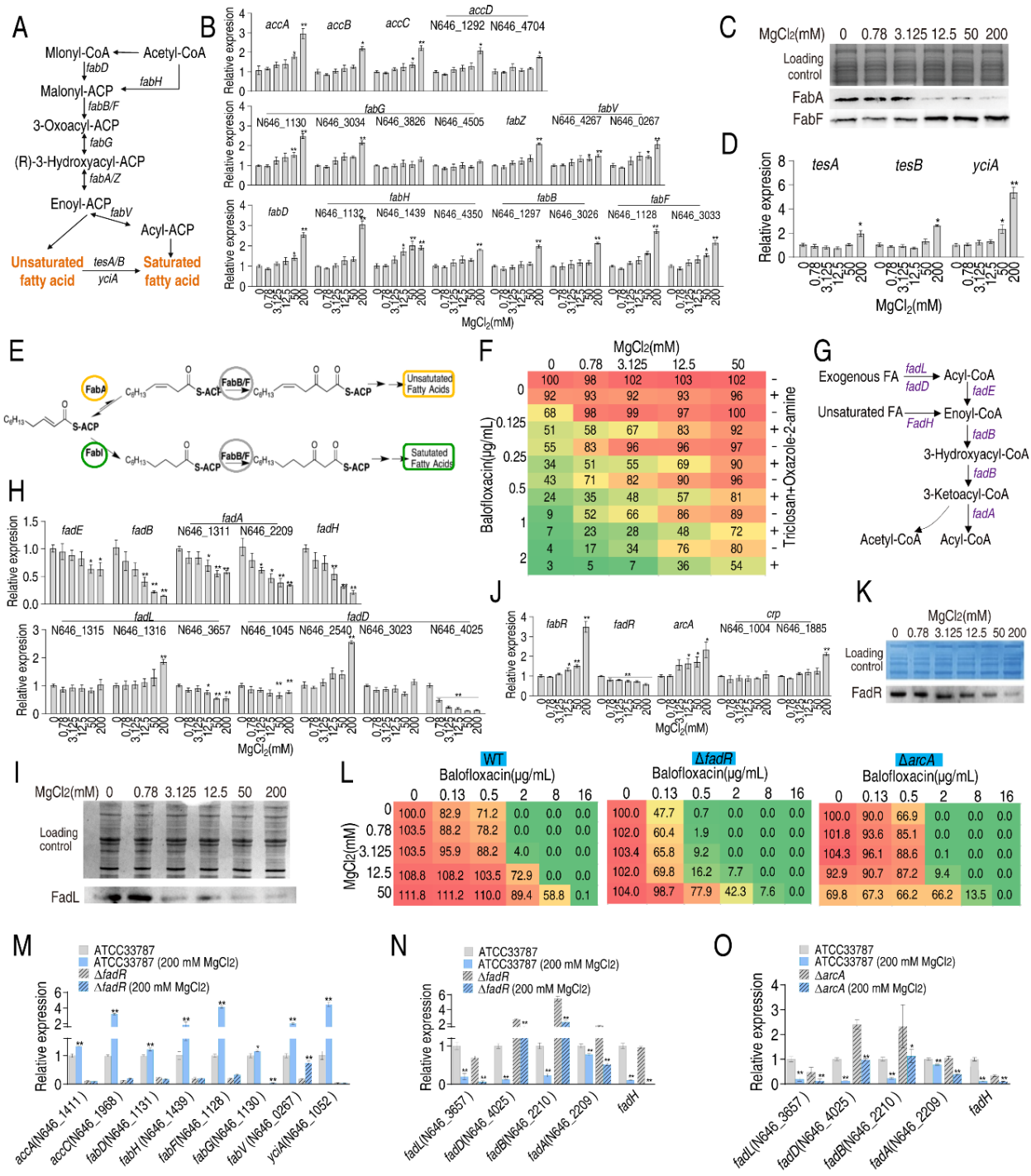

Figure 4 Mg^{2+} promotes biosynthesis of fatty acids. A. qRT-PCR for expression of fatty acid biosynthesis genes in the absence or presence of $MgCl_2$. **B.** Western blot for abundance of proteins responsible for conversion to unsatisfied fatty acid biosynthesis or satisfied fatty acid in the absence or presence of $MgCl_2$. **C.** qRT-PCR for expression of genes encoding conversion from unsatisfied fatty acid biosynthesis to satisfied fatty acid in the absence or presence of $MgCl_2$. **D.** Diagram for biosynthesis of saturated and

unsaturated acids. **E.** Synergy analysis for balofloxacin with triclosan + oxazole-2-amine for ATCC33787. Synergy is represented using a color scale or an isobologram, which compares the dose needed for 50% inhibition for synergistic agents (blue) and non-synergistic (i.e., additive) agents (red). **F.** Diagram for degradation of fatty acids. **G.** qRT-PCR for expression of genes encoding fatty acid degradation in the absence or presence of the indicated concentrations of $MgCl_2$. **H.** Western blot for abundance of FadL in the absence or presence of the indicated concentrations of $MgCl_2$. **I.** qRT-PCR for expression of regulatory genes of fatty acid biosynthesis in the absence or presence of the indicated concentrations of $MgCl_2$. **J.** Western blot for abundance of FadR in the absence or presence of the indicated concentrations of $MgCl_2$. **K** and **L.** Synergy analysis for $MgCl_2$ with BLFX for Δ*fadR* (L) and Δ*arcA* (M). Synergy is represented using a color scale or an isobologram, which compares the dose needed for 50% inhibition for synergistic agents (while) and non-synergistic (i.e., additive) agents (red). **M** , **N and O** qRT-PCR for expression of genes encoding biosynthesis of fatty acids and degradation of fatty acids (**M**) in ATCC33787 and Δ*fadR* **(N)** and Δ*arcA* **(O)**in the presence or absence of 200 mM $MgCl_2$.

$MgCl_2$ affects 16-carbon and 18-carbon fatty acid metabolism

To investigate the effect of Mg^{2+} on biosynthesis of saturated and unsaturated fatty acids, LC-MS was used to quantify 16-carbon and 18-carbon fatty acids, the main precursors for lipid biosynthesis (Zhang & Rock, 2008b). The abundance of saturated fatty acids, palmitic acid (C16:0), was increased, while the abundance of five unsaturated fatty acids, palmitoleic acid (C16:1), linoelaidic aid (C18:2), linoleic acid (C18:2), alpha-linoleic acid (C18:3), stearidonic acid (C18:4) was decreased with increasing $MgCl_2$ concentration (**Fig 5A**). The abundance of stearic acid (C16:0) and vaccenic acid (C18:1) was unaffected. Total saturated fatty acids increased and total

unsaturated fatty acids decreased with increasing Mg^{2+} (**Fig 5B**). These results support the conclusion that Mg^{2+} upregulates biosynthesis of saturated fatty acids but downregulates biosynthesis of unsaturated fatty acids.

Furthermore, direct exposure to palmitic acid inhibited balofloxacin-mediated killing (**Fig 3F**) but linolenic acid promoted balofloxacin-mediated killing in a dose-dependent manner (**Fig 5C**). Increasing exogenous palmitic acid and linolenic acid increased intracellular palmitic acid and linolenic acid, respectively (**Fig 5D**). When cells were co-treated with palmitic acid, linolenic acid, and balofloxacin, the effects of the two fatty acids appeared to be antagonistic as demonstrated by Bliss model (**Fig 5E** & **5F**). These results indicate that saturated and unsaturated fatty acids have antagonistic effects on balofloxacin resistance.

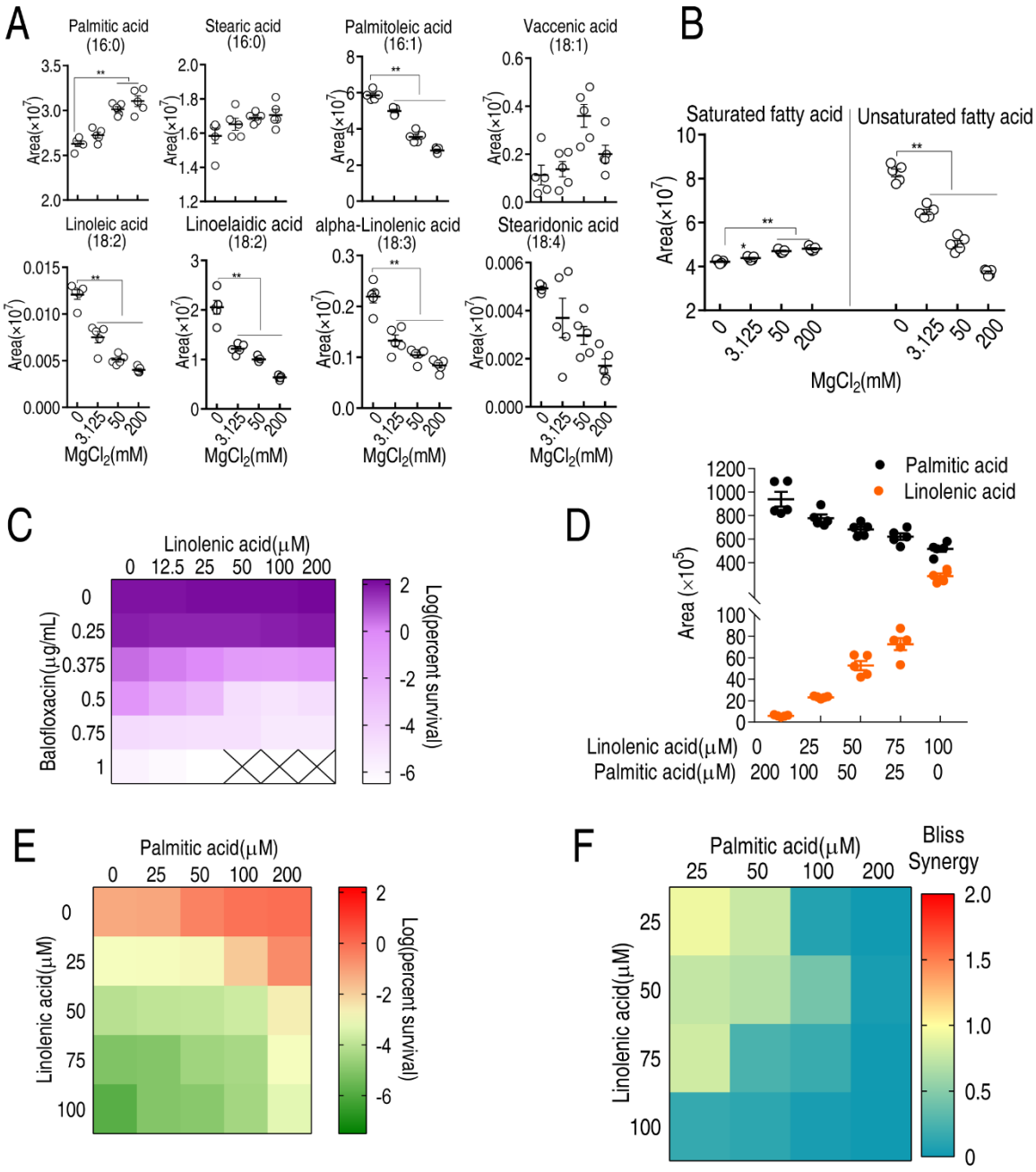

Figure 5. LC-MS targeted 16-carbon and 18-carbon fatty acids and role of palmitic acids and linolenic acids in BLFX resistance. A. Scatter plots of 16-carbon and 18-carbon fatty acids, detected by LC-MS. **B.** Scatter plots for total saturated fatty acid and unsaturated fatty acid with16-carbon and 18-carbon in data (**A**). **C.** Synergy analysis for BLFX with linolenic acid for ATCC 33787. Synergy is represented using a color scale or an isobologram, which compares the dose needed for 50% inhibition for synergistic agents (while) and non-synergistic (i.e., additive) agents (purple). **D.** LC-MS for abundance of intracellular linolenic acid and palmitic acid of ATCC 33787 in

synergy of the indicated exogenous linolenic acid and palmitic acid. **E.** Synergy analysis for linolenic acid with palmitic acid for BLFX-mediated killing to ATCC 33787. Synergy is represented using a color scale or an isobologram, which compares the dose needed for 50% inhibition for synergistic agents (blue) and non-synergistic (i.e., additive) agents (red). **F.** Bliss analysis in data **(E)**.

Mg^{2+} promotes phospholipid biosynthesis

Fatty acids are biosynthetic precursors of lysophosphatidic acid (LPA) and phosphatidic acid (PA), two key components of the cell membrane (Zhang & Rock, 2008a). Thus, LC-MS was used to profile the effect of Mg^{2+} on membrane lipid composition (**Fig EV6A**). Increasing concentration of Mg^{2+} increased the percentage of lipids increased from 61% to 67%, and saturated fatty acids from 24% to 26%, but decreased the percentage of unsaturated fatty acids from 15% to 8% (**Fig EV6B**). The abundance of 11 lipids, 32 lipids, and 53 were increased and of 26 lipids, 52 lipids, and 107 lipids were decreased in 3.125 mM, 50 mM, and 200 mM $MgCl_2$, respectively (**Fig 6C**). Saturated fatty acid and lipid increased and unsaturated fatty acid decreased in an Mg^{2+} dose-dependent manner (**Fig EV6D**). A total of 52 lipids were quantified, including 17 high abundance lipids (**Fig EV6E**). Phosphatidylethanolamine (PE) and phosphatidylglycerol (PG) were the first and second highest lipids in abundance (**Fig EV6E**) and PE decreased while PG increased with increasing Mg^{2+} (**Figs 6A**, **6B**). Similar effect was observed for unsaturated derivatives of PE and PG (**Fig 6C**). Principal component analysis (PCA) showed that component t [1] differentiates 0 and 3.125 mM Mg^{2+} from 50 and 200 mM Mg^{2+}, while component t [2] separates 50 mM Mg^{2+} from 0 and 200 mM Mg^{2+} and variants in 3.125 mM of Mg^{2+} treatment (**Fig 6D**).

S-plot analysis showed that upregulated lipids include behenic acid, PG[16:1(9Z)/16:1(9Z)], PG[18:2 (9Z, 12Z)/16:0], PA [14:0/22:6 (4Z, 7Z, 10Z, 13Z, 16Z, 19Z)], lysoPE(16:0/0:0) and downregulated lipids include linoelaidic acid, palmitoleic acid, PE-NMe(24:0/24:0), PE[16:0/14:1(9Z)], lysoPA(i-12:0/0:0) (**Fig 6E**). Among them, the abundance of PG[16:1(9Z)/16:1(9Z)], PG[18:2(9Z,12Z)/16:0], and behenic acid was increased, while that of linoelaidic acid, palmitoleic acid and PE[16:0/14:1(9Z)] were decreased with increasing Mg^{2+} (**Fig 6F**). Therefore, altered phospholipid abundance may play a role in the effect of Mg^{2+} on resistance to balofloxacin.

PE and PG are the two end products of phospholipid metabolism (**Fig 6G**). Expression of most genes in the phospholipid biosynthetic pathway, including *psd*, *pldB*, and *glpQ*, was increased in the presence of 200 mM $MgCl_2$, but not *pssA* and *etuB*, *etuC*, encoding the first enzyme and the last enzyme in the pathway, respectively. In addition, the expression of *gpsA*, encoding GpsA that transforms sn-glycerol-3P to glycerone-P, was increased in an independent of Mg^{2+} dose (**Fig 6H**). Phosphatidylglycerol phosphate synthase (PGS) encoded by *pgsA* and phosphatidylserine synthase (PSS) encoded by *pssA* are crucial enzymes for biosynthesis of PG and PE, respectively. Activities of PGS and PSS were elevated and reduced, respectively, by the increasing concentration of Mg^{2+} (**Fig 6I**). The effect of Mg^{2+} on the activity of PSS was confirmed with recombinant PSS (**Fig 6J**). The deletion of *plsB* and *pgpA*, the first and last genes for PG biosynthesis, respectively, lowered cell viability in the presence of balofloxacin (we

failed to obtain Δ*psd*) (**Figs 6K -I**). These results indicate that phospholipids may play a role in the effect of Mg^{2+} on resistance to balofloxacin; more specifically, PE may inhibit and PG may promote resistance to balofloxacin.

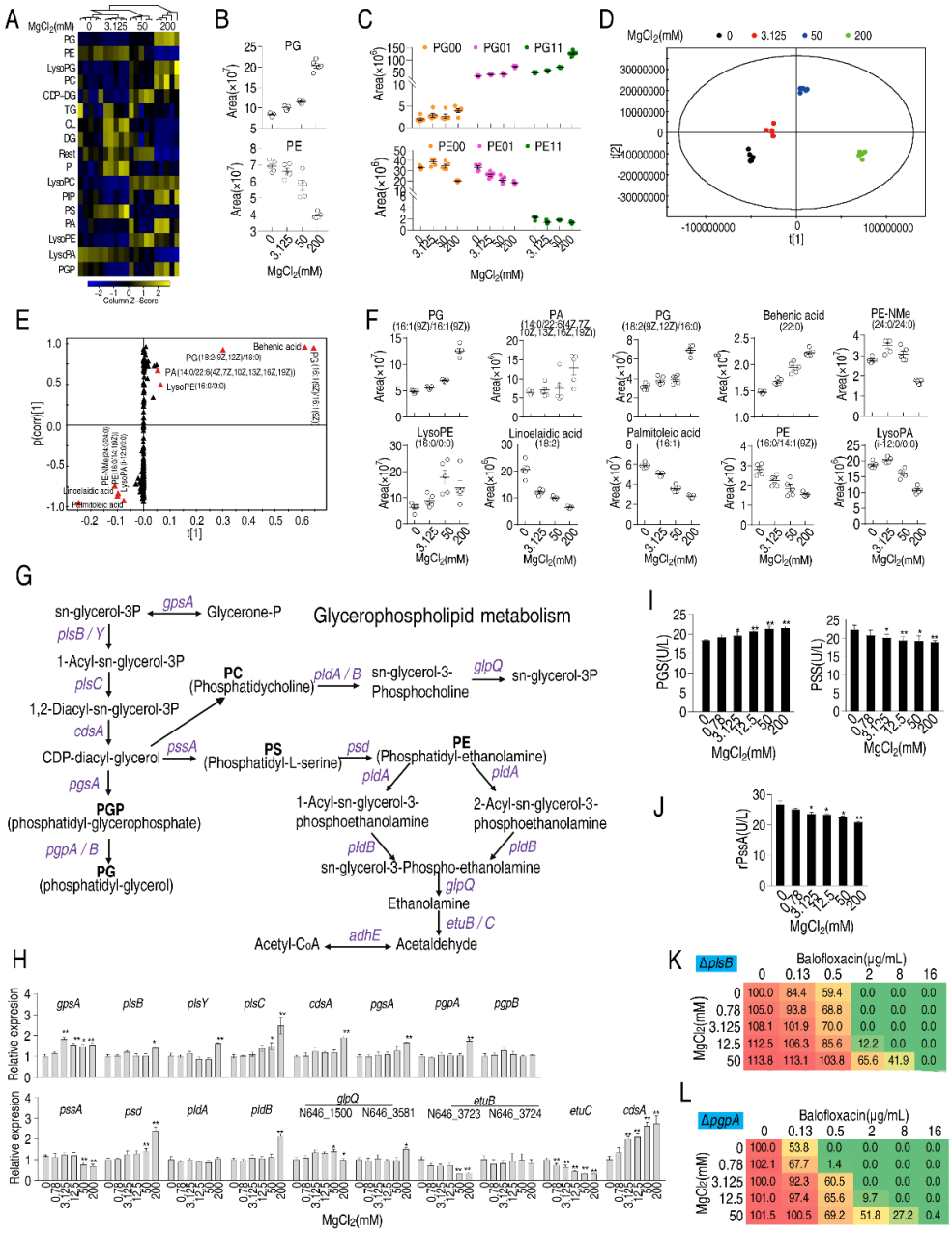

Figure 6 Effect of Mg2+ on phospholipid biosynthesis. A. Heatmap showing differential abundance of lipid. **B.** Abundance of ATCC33787 phosphatidylglycerol (PG) and phosphatidylethanolamine (PE) in the indicated concentrations of $MgCl_2$. **C.** Scatter plots of PG and PE with different saturation in the presence of the indicated

$MgCl_2$. **D.** PCA analysis of different concentrations of $MgCl_2$-induced phosphoglyceride metabolomes. Each dot represents the technical replicate of samples in the plot. **E.** S-plot generated from OPLS-DA. Predictive component p [1] and correlation *p* (corr) [1] differentiate 0 and 3.125 mM $MgCl_2$ from 50 and 200 mM $MgCl_2$. **F.** Scatter plot of biomarkers in data (**E**). **G.** Diagram showing phosphoglyceride metabolism. **H.** qRT-PCR for expression of genes encoding phosphoglyceride metabolism in the absence or the indicated concentrations of $MgCl_2$. **I.** Activity of PGS and PSS in the absence or presence of the indicated concentrations of $MgCl_2$. **J.** Activity of recombinant PSS in the absence or presence of the indicated concentrations of $MgCl_2$. **K** and **L** Synergy analysis for $MgCl_2$ with BLFX for Δ*plsB* (K) and Δ*pgpA* (L). Synergy is represented using a color scale or an isobologram, which compares the dose needed for 50% inhibition for synergistic agents (blue) and non-synergistic (i.e., additive) agents (red).

Mg^{2+} regulates membrane polarization, permeability and fluidity to confer balofloxacin resistance

Membrane potential and membrane polarization influence membrane permeability and uptake of antibiotics (Lee *et al.*, 2019; Peng *et al.*, 2015). Thus, we speculated that exogenous Mg^{2+} reduces membrane polarization. Here, we show that 12.5-200 mM $MgCl_2$ promotes membrane depolarization in a dose-dependent manner (**Fig 7A**). The effect of Mg^{2+} on proton motive force (PMF) displayed $MgCl_2$ dose- and time-dependent manner (**Fig 7B**). Specifically, membrane depolarization decreased over time without $MgCl_2$. However, depolarization gradually increased for 2 h, reached a plateau for 3 - 5 h and decreased from 5 to 10 h when supplemented with 0.78 or 3.125 mM $MgCl_2$. The extent of maximum depolarization and the length of time at higher level of depolarization also increased by $MgCl_2$ (**Figs 7C** and **7D**). These results suggest

that Mg^{2+} -dependent changes in membrane depolarization may influence bacterial resistance to antibiotics.

Moreover, efficacy of antibiotics is strongly influenced by bacterial membrane permeability and fluidity (Saeloh *et al*, 2018; Zhao *et al.*, 2021). Hence, membrane permeability and fluidity were investigated with fluorescence microscopy to visualize *V. alginolyticus* cells in the presence of FM5-95 (red dye) and various concentrations of $MgCl_2$. Mg^{2+} decreased red staining, and no staining was observed in the presence of 200 mM Mg^{2+} (**Fig 7D**). Consistently, the uptake of SYTO9 dye decreased with increasing $MgCl_2$, indicating bacterial membrane permeability decreased in an Mg^{2+} dose-dependent manner (**Fig 7E**). These results indicate that exogenous Mg^{2+} decreased bacterial membrane permeability.

Furthermore, exogenous palmitic acid shifted the fluorescence signal peaks to the left in an $MgCl_2$- and palmitic acid concentration-dependent manner (**Fig 7F**). In contrast, exogenous linolenic acid shifted the peak to the right in a dose-dependent manner (**Fig 7G**). These results support the conclusion that exogenous palmitic acid and linolenic acid decrease or increase membrane permeability, respectively. In Δ*fadR* cells, membrane permeability increased and then slowly decreased with increasing Mg^{2+}, remaining higher than the control (**Fig 7H**). However, Δ*arcA* cells displayed reduced membrane permeability in the presence of low but not high $MgCl_2$ (**Fig 7I**). Δ*pgpA* cells exhibited higher membrane permeability than control cells at all $MgCl_2$

concentrations, but the effect was smaller at higher $MgCl_2$ (**Fig 7J**). These data are consistent with the viability of these mutants as described above (**Figs 4L** and **6L**).

Relative membrane permeability appeared to correlate with relative intracellular balofloxacin and antibiotic efficacy. Exogenous palmitic acid and linolenic acid reduced and promoted uptake of balofloxacin 159- and 18-fold, respectively (**Fig 7K**). Loss of *fadR* and *pgpA* increased intracellular balofloxacin (**Fig 7K**). These data suggest that bacterial membrane permeability is a critical factor in the efficacy and uptake of balofloxacin, in the presence or absence of exogenous $MgCl_2$.

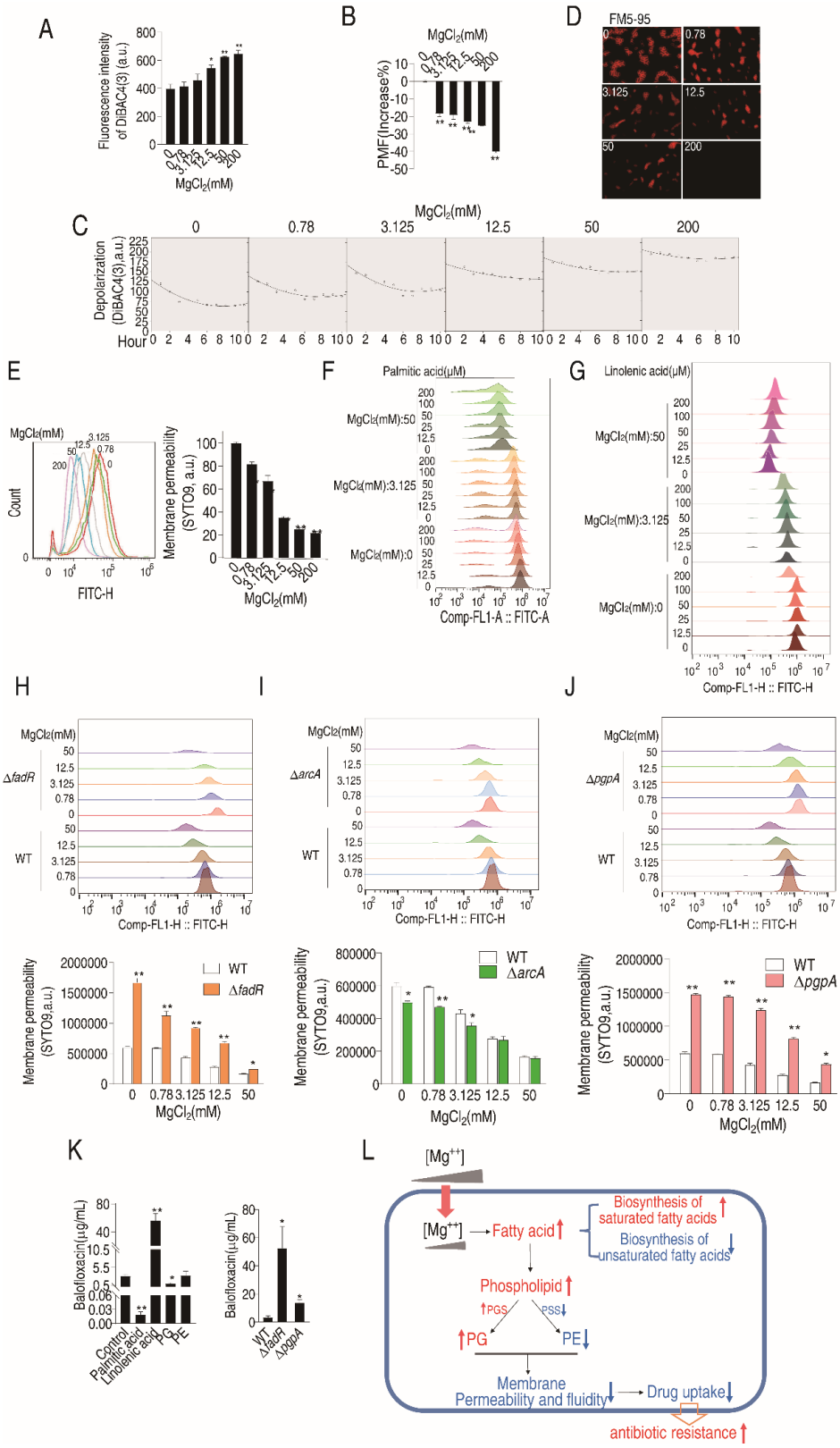

Figure 7. Mg^{2+} regulates membrane polarization, permeability and fluidity to confer balofloxacin resistance. A and **B**. Depolarization **(A)** and PMF **(B)** of ATCC33787 in the absence or indicated concentrations of $MgCl_2$. **C** and **D**. Dynamic depolarization (**D**) Membrane fluidity of ATCC33787 in the absence or presence of the

indicated concentrations of $MgCl_2$, detected in fluorescence microscopy. **E.** Membrane permeability of ATCC33787 in the absence or presence of the indicated concentrations of $MgCl_2$. **F** and **G**. Membrane permeability of ATCC33787 cultured in palmitic acid **(F)** or linolenic acid **(G)** in the indicated concentrations of $MgCl_2$. **H** and **I**. Membrane permeability of Δ*fadR* **(H)** and Δ*arcA* **(I)** in the absence or presence of the indicated concentrations of $MgCl_2$. **J.** Membrane permeability of Δ*pgpA* in the absence or presence of the indicated concentrations of $MgCl_2$. **K.** Intracellular BLFX of ATCC33787 in the presence of palmitic acid, linolenic acid, PG, and PE (lefe panel) or in Δ*fadR* and Δ*pgpA* mutants (right panel). **L.** Diagram for mechanisms by which Mg^{2+}-mediated resistance to BLFX.

Discussion

The present study explores the effect of Mg^{2+} on phenotypic in *V. alginolyticus*. The results suggest that exogenous Mg^{2+} promotes biosynthesis of saturated fatty acids and inhibits biosynthesis of unsaturated fatty acids, while it also upregulates the activity of PGS and the abundance of PG, and downregulates the activity of PSS and abundance of PE. As a result, membrane permeability and antibiotic uptake decrease (**Fig 7L**), enabling phenotypic resistance. The results are consistent with the observed impact of exogenous Mg^{2+} on bacterial survival in the presence of balofloxacin and other antibiotics, and it is well recognized that membrane permeability critically impacts drug efficacy. Another pathway that influences drug uptake involves glutamine-inosine transport mediated by CpxA/R-OmpF (Zhao *et al.*, 2021). The results also show that exogenous fatty acids influence membrane permeability and bacterial survival in the presence of balofloxacin.

Mg^{2+} is the most abundant divalent cation in the cell (Pohland & Schneider, 2019; Pontes *et al*, 2015) and it plays many essential roles. For example, Mg^{2+} stabilizes macromolecular complexes and membranes, binds cytoplasmic nucleic acids and nucleotides, interacts with phospholipid head groups and cell surface molecules, and is an essential cofactor in many enzymatic reactions (Groisman *et al*, 2013). A novel observation of the present study is that exogenous Mg^{2+} influences the abundance of palmitic acid and linolenic acid and that it upregulates PGS and downregulates PSS. These findings extend our understanding of the complexity of the biological functions of the divalent magnesium cation.

Recent studies suggest a link between fatty acid biosynthesis and antibiotic resistance in *E. tarda* (Su *et al*, 2021). The present study shows that Mg^{2+} has opposite effects on the abundance of saturated and unsaturated fatty acids, stimulating biosynthesis of saturated fatty acids at moderately high levels, while inhibiting biosynthesis of unsaturated fatty acids at ≥ 3 mM Mg^{2+}. Therefore, ratio of saturated and unsaturated fatty acids should be a key clue to understand antibiotic resistance.

In previous studies of gram-positive and gran-negative bacteria (Kumariya *et al*, 2015; Said *et al*, 1987), it was shown that 10 - 20 mM Mg^{2+} disrupts *Staphylococcus aureus* membranes and kills stationary-phase *S. aureus* cells, but it does influence survival of *Escherichia coli* and *Bacillus subtilis (Xie & Yang, 2016)*. Low concentrations of Mg^{2+} (≤ 10 mM) induce PmrAB-dependent modification of lipid A in wild-type *E. coli* (Herrera *et al*, 2010). A putative zwitterionic amino-containing phospholipid increased significantly, whereas amounts of phosphatidylglycerol and cardiolipin decreased in

two mutants of *Enterococcus faecium* resistant to mundticin KS (Sakayori *et al*, 2003). However, Mg^{2+} induces antibiotic resistance through regulating the activity of PGS and PSS is not reported. More importantly, the regulation targets the two enzymes in a reverse manner to enlarge the change in the ratio between PE and PG for recognition of antibiotic resistance, which is a previously unknown mechanism mediated by Mg^{2+}. Previous studies on membrane permeability also show that PhoP/Q is activated by low magnesium, and that inhibition or inactivation of PhoP/Q stimulates uptake of β-lactam antibiotics in *Stenotrophomonas maltophilia* (Huang *et al*, 2021). The effects of the outer membrane permeabilizers, polymyxin B nonapeptide and EDTA, are completely abolished by 3 mM Mg^{2+} (Kwon & Lu, 2006). In response to Mg^{2+} limited growth, enteric Gram-negative bacteria show higher acylation of lipid A, which alters membrane permeability and reduces uptake of cationic antimicrobial peptides (Guo *et al*, 1998). Mg^{2+} reverts the high sensitivity of rough mutants of *Salmonella typhimurium*, *S. minnesota*, and *Escherichia coli* 08 (i.e. with defects in the carbohydrate core of the lipopolysaccharide) to several antibiotics (Stan-Lotter *et al*, 1979). Mg^{2+} (1 mM) totally inhibited aminoglycoside-mediated outer membrane permeabilization in *Pseudomonas aeruginosa* (Hancock *et al*, 1981). However, mechanisms underlying Mg^{2+} regulation to antibiotic resistance are largely unknown. The present study reveals that Mg^{2+} plays the crucial role in the membrane permeability responsible for antibiotic resistance via modulating PE and PG in phospholipid metabolism.

In summary, the present study shows that Mg^{2+} modulates the phenotypic resistance of *V. alginolyticus* to balofloxacin and potentially other quinolones and other classes of

antibiotics by a mechanism that involves altered membrane permeability and reduced antibiotic uptake. These findings inform the ongoing and future search for ways to improve the therapeutic effects of antibiotics to magnetism-induced phenotypic resistance.

Materials and Methods

Bacterial strains and culture

V. alginolyticus ATCC33787 and *V. parahaemolyticus* 01 are from our laboratory collection (Jiang *et al*, 2022; Kou *et al*, 2022). They were cultured in 0.5% yeast broth (HuanKai Microbial, Guangdong, China) (pH 7.0) with 3% NaCl at 30 °C overnight. The cultures were diluted 1:50 (v/v) and grown in fresh 0.5% yeast broth supplemented with desired concentrations of $MgCl_2$ at 30 °C until OD600 = 0.6. Bacteria were harvested by centrifugation at 8,000 rpm for 3 min and resuspended in corresponding concentrations of $MgCl_2$ to 0.6 of OD600.

Measurement of the minimum inhibitory concentration (MIC) by microtitre-dilution-method

MIC using microtitre-dilution-method was performed as previously described (Zhang *et al*, 2019). In brief, the overnight bacterial cultures in 3% NaCl were diluted at 1:100 (v/v) in fresh 0.5% yeast broth supplemented with desired concentrations of $MgCl_2$, cultured at 30 °C and collected when the cells arrived at an OD600 of 0.6 in medium without $MgCl_2$. Then, 1 X 10^5 CFU cells were dispensed into each well of a 96-well microtiter polystyrene tray after which a series of 2-fold dilutions of antibiotic was

added. Following incubation at 30 °C for 16 h, the MIC was defined as the lowest antibiotic concentration that inhibited visible growth. Three biological repeats were carried out.

Measurement of MIC by Oxford method

Determination of MIC by Oxford cup was performed as previously described (Liu *et al*, 2015). Bacterial cells cultured overnight in yeast medium were diluted at 1:100, shaken at 30 ^{0}C and 200 rpm until the OD_{600} nm reached at 0.6. Aliquot of 100 μL cells were spread on 0.5% yeast solid medium containing 3% NaCl and 0, 0.625, 1.25, 2.5, 5, 10, 20, or 40 mM of $MgCl_2$. Oxford cups were placed on the solid medium, and various amounts of balofloxacin (0, 0.39, 0.78, 1.56, 3.125, 6.25, and 12.5 μg) were added. After culturing at 30 °C for 12 h, diameter of the inhibition zone was measured and the inhibition area was calculated.

Measurement of intracellular balofloxacin

Measurement of intracellular balofloxacin was performed by LC-MS analysis and plate-counting assay. For LC-MS analysis, ATCC33787 cultured in the desired concentrations of $MgCl_2$ were collected and adjusted to OD 0.6. Aliquot of 50 mL bacterial cells were added into a 250 mL Erlenmeyer flask and then 300 μL of 10 mg/mL balofloxacin (final concentration is 60 μg/mL). After being cultured for 6 h at 30 °C, these bacterial cells were collected and adjusted to OD 1.0 with 3% NaCl containing corresponding concentrations of $MgCl_2$. Aliquot of 30 mL bacteria were

collected and washed three times using mobile phase (acetonitrile: double distilled water containing 0.1mol/l formic acid = 35:65) for LC-MS detection. The bacterial cells were added 1 mL mobile phase, crushed in ice water bath for 10 min (crush for 2S, pause for 3S at 35% power). Following by centrifugation, supernatants were collected, filtered, and then measured by using liquid chromatography for balofloxacin. Different concentrations of balofloxacin were used for a standard curve. For plate-counting assay, ATCC33787 cells cultured overnight were diluted at 1:100, shaken at 30 ^{0}C and 200 rpm until the OD_{600} nm reached at 0.6. The cells were diluted at 1:100 and spread on LB agar to preparing ATCC33787 plates. Meanwhile, ATCC33787 cells were cultured in medium with desired $MgCl_2$ and at 30 °C and 200 rpm for 6 h. These cells were collected, washed and sonicated. The sonicated solution was added to Oxford cups with the ATCC33787 plates. After culturing at 30 °C for 12 h, diameter of the inhibition zone was measured. A gradient of balofloxacin was used as a standard curve for drug quantification.

Measurement of intracellular magnesium

Measurements of intracellular Mg^{2+} concentration were carried out as previously described with a modification (Yang *et al.*, 2018). In brief, *V. alginolyticus* cultured in 0%, 0.78%, 3.125%, 12.5%, 50%, and 200% $MgCl_2$ were collected, washed, and resuspended in the same concentrations of $MgCl_2$ to an OD600 of 1.0. Aliquots of 20 mL of bacterial suspensions were centrifuged and washed by ddH_2O once. The resulting cells were weighted, which was designated wet weight. These samples were freeze-

dried overnight, which was designated dry weight. Intracellular water volume was calculated using the following formula: W × (1-W/D-0.23) as described previously (Unemoto *et al*, 1973). Two hundred microliters of concentrated nitric acid was added to the dried cells and then heated in 75 °C for 20 min. After diluting the samples 20-fold, they were analyzed for Mg^{2+} concentration by inductively coupled plasma mass spectrometry (ICP-MS) (iCAP 6500, Thermo Fisher). The intracellular Mg^{2+} concentration was calculated according to the volume of intracellular water.

Western blotting

Western blotting was carried out as described previously (Yao *et al*, 2019). Bacterial protein samples were prepared by ultrasound treatment, resolved on a 12% SDS-PAGE and transferred to nitrocellulose membranes (GE Healthcare Life Sciences). The membranes were incubated with 1:100 of the primary mouse antibodies, followed by goat anti-mouse secondary antibodies conjugated with horseradish peroxidase. Band intensities were detected by using a chemiluminescence imaging analysis system, Tanon-5200.

Metabolomics analysis

Metabolomics analysis was performed by GC-MS as described previously (Yang *et al.*, 2018). Briefly, ATCC33787 were cultured in 0.5% yeast broth with desired $MgCl_2$. Equivalent numbers of cells were quenched with 60% (v/v) cold methanol (Sigma) and then centrifuged at 8,000 rpm at 4 °C for 5 min. One milliliter of cold methanol was

used to extract metabolites. To do this, the samples were sonicated for 5 min at a 10-Wpower setting using the Ultrasonic Processor (JY92-IIDN, Scientz, China), followed by centrifugation at 12,000 rpm in 4 °C for 10 min. Supernatants were collected and 10 μL ribitol (0.1 mg per mL, Sigma-Aldrich, USA) was added into each sample as an internal quantitative standard. The supernatants were concentrated for metabolite derivatization and then used for GC-MS analysis. Every experiment was repeated by five biological replicates. GC-MS detection and spectral processing for GC-MS were carried out using the Agilent 7890A GC equipped with an Agilent 5975C VL MSD detector (Agilent Technologies, USA) as described previously (Unemoto *et al.*, 1973; Yang *et al.*, 2018). Statistical difference was obtained by Kruskal Wallis test and Manne Whitney test using SPSS 13.0 and a p value < 0.01 was considered significant. Hierarchical clustering was completed in the R platform (https://cran.r-project.org/) with the function "heatmap. 2" of "gplots library". Z score analysis was used to scale each metabolite. Multivariate statistical analysis included principal component analysis (PCA) and orthogonal partial least square discriminant analysis (OPLS-DA) implemented with SIMCA 12.0 (Umetrics, Umeå, Sweden). Control scaling was selected prior to fitting. All variables were mean centered and scaled to pareto variance of each variable. PCA was used to reduce the high dimension of the data set. Differential metabolites to their respective biochemical pathways were outlined in the MetaboAnalyst 3.0 (http://www.metaboanalyst.ca/). Pathways were enriched by raw p value < 0.05.

qRT-PCR

Quantitative real time polymerase chain reaction (qRT-PCR) was carried out as described previously (Yang *et al*, 2020). Total RNA was extracted from *V. alginolyticus* using TRIZOL regent (Invitrogen Life Technologies) according to the protocol. RNA Electrophoresis was carried out in 1% (w/v) agarose gels to identify quality of the extracted RNA. By using a PrimeScriptTM RT reagent Kit with gDNA eraser (Takara, Japan), reverse transcription-PCR was carried out on 1 μg of total RNA and primers are listed in **Table EV2.** qRT-PCR was performed in 384-well plates with a total volume of 10 μL and the reaction mixtures were run on a LightCycler 480 system (Roche, Germany). Data are shown as the relative mRNA expression compared to 0% $MgCl_2$ test with the endogenous reference 16S rRNA gene.

Antibiotic bactericidal assay

Antibiotic bactericidal assay was performed as described previously with a modification (Li *et al*, 2016; Zhao *et al.*, 2021). The cultured bacteria of ATCC33787 and its mutant strains were transferred to fresh yeast medium at a dilution of 1:1000 and dispensed into test tubes and then the indicated concentrations of $MgCl_2$ and balofloxacin were added. If desired, 2 mM 2-aminooxazole and 1 μg/mL triclosan were or a metabolite complemented. These mixtures were incubated at 30 °C and 200 rpm for 6 h. Cells were collected. To determine CFU per mL, 100-μL samples were 10-fold serially diluted with 900 μL M9 buffer and an aliquot of 5 μL of each dilution was spotted onto the LB agar plates and cultured at 30 °C for 8 h.

Construction of gene-deleted mutants

Construction of gene-deleted mutants was carried out as described previously (Kuang *et al*, 2021). Primers were designed as shown in **Table EV3** using CE Design V1.03 software. To construct gene-deleted mutants, upstream and downstream 500-bp fragments were amplified from the genome using two pairs of primers (primers P1 and P2, primers P3 and P4), and then merged into a 1,000-bp fragment by overlap PCR using a pair of primers (primers P1 and P4). After the fragments were digested by *Xba*I, they were ligated into the pDS132 vector digested by the same enzymes, transformed into MC1061 competent cells. Conversion products were coated on LB plate containing 25 μg/mL chloramphenicol and cultured at 37 °C overnight. The plasmids from colony growing on the plate were identified by PCR using a pair of primers (primers P1 and P4) and sequenced. The sequenced plasmids were transformed into MFD λ pir competent cells as donor. MFD λpir and recipient bacterium ATCC 33787 were cultured to an optical density (OD) of 1.0 and then mixed at a ratio of 4:1. After centrifugation, the pellets were resuspended with 50 μL LB medium including DAP (100 μg/mL), dropped onto sterilized filter paper on LB medium including DAP (100 μg/mL), and cultured for 16-18 h at 37 °C.

All bacteria rinsed from the filter paper with LB medium were smeared onto the LB plate with chloramphenicol (25 μg/mL) and Ampicillin (100 μg/mL). After cultured for 16-18 h at 37 °C, bacteria were screened by LB plate with above two antibiotics. The bacteria were identified by plasmid PCR using a pair of primers P1 and P4 and

sequencing and then were cultured and smeared onto the LB plates with 20% sucrose. The clones were cultured and smeared onto the LB plates with 20% sucrose again. The clones, which did not grow on the LB plates with chloramphenicol but grew on the LB plates with 20% sucrose, were identified by PCR using primer P7P8 (primer P7 is set at about 250 bp upstream of P1, and primer P8 is set at about 250 bp downstream of P4), P4P7, and P5P6 (for amplification of the target gene).

LC-MS analysis for lipidomics

ATCC33787 were cultured in medium with desired concentrations of $MgCl_2$, washed by 3% NaCl with the desired concentrations of $MgCl_2$, and adjusted to OD 1.0. Aliquot of 30 mL the cultures was centrifuged each sample and bacterial cells were collected. Aliquot of 800 μL distilled water was added and treated for 5 min at 100 °C to inactivate phospholipase C. Protein concentration was determined with BCA kit. Sample solution with 3 mg protein was transferred into a 10 mL centrifuge tube, and supplemented with distilled water to 800 μL. Then all samples were processed as follows: 1 mL chloroform and 2 mL methanol (to make the volume ratio of chloroform: methanol: water = 1:2 : 0.8) were added and cholic acid was as an internal standard; These mixtures were vortexed for 2 min and then 1 mL chloroform was add and vortex for 30s; 1 mL 10% NaCl solution was add, vortexed for 30s, and placed at room temperature overnight. After the solution was layered, a 2.5 mL syringe was used to suck the lowest layer (chloroform layer) to a new EP tube. Solution of the chloroform layer was evaporated in the rotary evaporator for 2 h and then 1 mL mobile phase (50% and 50%B. A, 25

mM ammonium acetate / methanol (30 : 70); B, methanol) was added for analysis of lipids by LC-MS. Database (https://hmdb.ca) was used for lipid identification.

Measurement of enzyme activity

Enzyme activity was carried out as previously described (Jiang *et al*, 2020). Cells cultured in medium were collected and washed three times with saline. The bacterial cells were suspended in Tris–HCl (pH 7.4) and disrupted by sonic oscillation for 6 min (200 W total power with 35% output, 2 s pulse, 3 s pause over ice). After centrifugation, supernatants were collected. The protein concentration of the supernatant was determined using Bradford assay (Beyotime, P0009). Then, 200 μg proteins were used for determination of pyruvate dehydrogenase (PDH), α-ketoglutarate dehydrogenase (KGDH) and succinate dehydrogenase (SDH) activity.

Measurement of proton motive force

Measurement of the transmembrane voltage delta PSI (δPSI), which is the electrical component of the PMF, was performed as previously described (Cheng *et al*, 2018). Bacteria cultured in medium with desired concentrations of $MgCl_2$ were collected at centrifugation and labeled by DiO2(3). Approximately 1×10^7 CFU were added to a flow cytometry tube containing 1 mL buffer with 10 μM DiOC2(3) (Sigma) and incubated in the dark for 30 min at 30 ^{0}C. Samples were assayed with BD FACSCalibur flow cytometer with a 488 nm excitation wavelength. Gates for bacterial populations were based on the control population by using forward versus side scatter and red versus

green emission. Size and membrane potential determined the intensity of Red (488 nm excitation, 610 nm emission) fluorescence. The diverse ratios of red and green indicated fluorescence intensity values of the gated populations. Computational formula of membrane potential: $\mathrm{Log}(10^{3/2} \times (\frac{\text{red fluorescence}}{\text{green fluorescence}}))$.

Measurement of depolarization

The membrane potential was estimated by measuring the fluorescence of the potential-dependent probe DiBAC4(3) (Saint-Ruf *et al*, 2016). ATCC33787 were cultured in medium with desired concentrations of $MgCl_2$, collected and then adjusted to OD 0.6. Aliquot of 100 μL bacterial cells were diluted to 1 mL, and 2 μL of 5 mM DiBAC4(3) was added. After incubated for 15 min at 30 ℃ without light and vibration, these samples were filtered and detected by BD FACSCalibur.

Measurement of fluidity by fluorescence microscopy

ATCC33787 were cultured in medium with desired concentrations of $MgCl_2$, collected and then adjusted to OD 0.6. Aliquot of 100 μL bacteria cells of each sample were diluted to 1 mL and 10 μL (10 mg/mL) FM5-95 was added. After incubated for 20 min at 30 ℃ at vibration without light, the sample was centrifuged for 10 min at 12,000 rpm. The pellets were resuspended with 20 μL of 3% NaCI. Aliquot of 2 μL sample was dropped on the agarose slide, and take photos under the inverted fluorescence microscope.

Measurement of membrane permeability

Measurement of membrane permeability was carried out as described previously (Su *et al.*, 2021). ATCC33787 were cultured in medium with desired concentrations of $MgCl_2$, collected and then adjusted to OD 0.6. Aliquot of 100 μL bacteria cells of each sample were diluted to 1 mL and 2 μL 10 mg/mL SYT09 was added. After incubated for 15 min at 30 ℃ at vibration without light, the mixtures were filtered and measured by BD FACSCalibur.

Acknowledgments

This work is sponsored by International Cooperation and Exchange program of National Natural Science Foundation of China (32273177) (to P.B.), Innovation Group Project of Southern Marine Science and Engineering Guangdong Laboratory (Zhuhai) 311020006 (to P.B.), Natural Science Foundation of Guangdong Province 2022A1515012079 (L. H.) and the Science and Technology Planning Project of Guangdong Province (No. 2023B1212060028).

Author Contributions

B. Peng conceived the idea, designed the experiments and supervise the projects. H. Li and J. Yang, S.F. Kuang conducted the experiments, and interpreted the results.

Declaration of interest statement

Authors declare that they have no competing interests.

References

Booth SC, Workentine ML, Wen J, Shaykhutdinov R, Vogel HJ, Ceri H, Turner RJ, Weljie AM (2011) Differences in metabolism between the biofilm and planktonic response to metal stress. *J Proteome Res* 10: 3190-3199

Cheng ZX, Yang MJ, Peng B, Peng XX, Lin XM, Li H (2018) The depressed central carbon and energy metabolisms is associated to the acquisition of levofloxacin resistance in Vibrio alginolyticus. *J Proteomics* 181: 83-91

Ciofu O, Moser C, Jensen PO, Hoiby N (2022) Tolerance and resistance of microbial biofilms. *Nat Rev Microbiol* 20: 621-635

Corona F, Martinez JL (2013) Phenotypic Resistance to Antibiotics. *Antibiotics (Basel)* 2: 237-255

Deitchman AN, Singh RSP, Rand KH, Derendorf H (2018) Enhanced in vitro activity of tigecycline in the presence of chelating agents. *Int J Antimicrob Ag* 51: 799-802

Du J, Zhu M, Bao HK, Li B, Dong YL, Xiao CJ, Zhang GY, Henter I, Rudorfer M, Vitiello B (2016) The Role of Nutrients in Protecting Mitochondrial Function and Neurotransmitter Signaling: Implications for the Treatment of Depression, PTSD, and Suicidal Behaviors. *Crit Rev Food Sci* 56: 2560-2578

Feng YJ, Cronan JE (2010) Overlapping Repressor Binding Sites Result in Additive Regulation of Escherichia coli FadH by FadR and ArcA. *J Bacteriol* 192: 4289-4299

Fujita Y, Matsuoka H, Hirooka K (2007) Regulation of fatty acid metabolism in bacteria. *Mol Microbiol* 66: 829-839

Garfinkel L, Garfinkel D (1985) Magnesium regulation of the glycolytic pathway and the enzymes involved. *Magnesium* 4: 60-72

Groisman EA, Hollands K, Kriner MA, Lee EJ, Park SY, Pontes MH (2013) Bacterial Mg2+ Homeostasis, Transport, and Virulence. *Annu Rev Genet* 47: 625-646

Guo L, Lim KB, Poduje CM, Daniel M, Gunn JS, Hackett M, Miller SI (1998) Lipid A acylation and bacterial resistance against vertebrate antimicrobial peptides. *Cell* 95: 189-198

Hancock RE, Raffle VJ, Nicas TI (1981) Involvement of the outer membrane in gentamicin and streptomycin uptake and killing in Pseudomonas aeruginosa. *Antimicrob Agents Chemother* 19: 777-785

Herrera CM, Hankins JV, Trent MS (2010) Activation of PmrA inhibits LpxT-dependent phosphorylation of lipid A promoting resistance to antimicrobial peptides. *Mol Microbiol* 76: 1444-1460

Huang HH, Wu BK, Li LH, Lin YT, Yang TC (2021) Role of the PhoPQ two-component regulatory system in the beta-lactam resistance of Stenotrophomonas maltophilia. *J Antimicrob Chemoth* 76: 1480-1486

Jiang M, Chen ZG, Li H, Zhang TT, Yang MJ, Peng XX, Peng B (2022) Succinate and inosine coordinate innate immune response to bacterial infection. *Plos Pathog* 18

Jiang M, Kuang SF, Lai SS, Zhang S, Yang J, Peng B, Peng XX, Chen ZG, Li H (2020) Na+-NQR Confers Aminoglycoside Resistance via the Regulation of L-Alanine Metabolism. *Mbio* 11

Jiang M, Su YB, Ye JZ, Li H, Kuang SF, Wu JH, Li SH, Peng XX, Peng B (2023) Ampicillin-controlled glucose metabolism manipulates the transition from tolerance to resistance in bacteria. *Sci Adv* 9: eade8582

Kobylka J, Kuth MS, Mueller RT, Geertsma ER, Pos KM (2020) AcrB: a mean, keen, drug efflux machine. *Ann Ny Acad Sci* 1459: 38-68

Kou TS, Wu JH, Chen XW, Chen ZG, Zheng J, Peng B (2022) Exogenous glycine promotes oxidation of glutathione and restores sensitivity of bacterial pathogens to serum-induced cell death. *Redox Biol* 58

Kuang SF, Feng DY, Chen ZG, Liang ZZ, Xiang JJ, Li H, Peng XX, Zhang TT (2021) Inactivation of Nitrite-Dependent Nitric Oxide Biosynthesis Is Responsible for Overlapped Antibiotic Resistance between Naturally and Artificially Evolved Pseudomonas aeruginosa. *Msystems* 6

Kumariya R, Sood SK, Rajput YS, Saini N, Garsa AK (2015) Increased membrane surface positive charge and altered membrane fluidity leads to cationic antimicrobial peptide resistance in Enterococcus faecalis. *Bba-Biomembranes* 1848: 1367-1375

Kwon DH, Lu CD (2006) Polyamines increase antibiotic susceptibility in Pseudomonas aeruginosa. *Antimicrob Agents Ch* 50: 1623-1627

Lee DD, Galera-Laporta L, Bialecka-Fornal M, Moon EC, Shen Z, Briggs SP, Garcia-Ojalvo J, Suel GM (2019) Magnesium Flux Modulates Ribosomes to Increase Bacterial Survival. *Cell* 177: 352-360 e313

Lee HH, Collins JJ (2012) Microbial environments confound antibiotic efficacy. *Nat Chem Biol* 8: 6-9

Li WX, Yao ZJ, Sun LN, Hu WJ, Cao JJ, Lin WX, Lin XM (2016) Proteomics Analysis Reveals a Potential Antibiotic Cocktail Therapy Strategy for Aeromonas hydrophila Infection in Biofilm. *J Proteome Res* 15: 1810-1820

Liu XJ, Zhu WC, Su YB, Guo C, Zeng ZH, Zhu H, Li H, Peng XX (2015) Characterization of ampicillin-stressed proteomics and development of a direct method for detecting drug-binding proteins in Edwardsiella tarda. *J Proteomics* 116: 97-105

Lu J, Wang Y, Jin M, Yuan ZG, Bond P, Guo JH (2020) Both silver ions and silver nanoparticles facilitate the horizontal transfer of plasmid-mediated antibiotic resistance genes. *Water Res* 169

Lunestad BT, Goksøyr J (1990) Reduction in the antibacterial effect of oxy-tetracycline in sea water by complex formation with magnesium and calcium. *Dis aquat Org* 9: 67-72

Peng B, Su YB, Li H, Han Y, Guo C, Tian YM, Peng XX (2015) Exogenous Alanine and/or Glucose plus Kanamycin Kills Antibiotic-Resistant Bacteria. *Cell Metab* 21: 249-261

Pohland AC, Schneider D (2019) Mg2+ homeostasis and transport in cyanobacteria - at the crossroads of bacterial and chloroplast Mg2+ import. *Biol Chem* 400: 1289-1301

Pontes MH, Sevostyanova A, Groisman EA (2015) When Too Much ATP Is Bad for Protein Synthesis. *J Mol Biol* 427: 2586-2594

Poole K (2017) At the Nexus of Antibiotics and Metals: The Impact of Cu and Zn on Antibiotic Activity and Resistance. *Trends Microbiol* 25: 820-832

Saeloh D, Tipmanee V, Jim KK, Dekker MP, Bitter W, Voravuthikunchai SP, Wenzel M, Hamoen LW (2018) The novel antibiotic rhodomyrtone traps membrane proteins in vesicles with increased fluidity. *Plos Pathog* 14

Said AA, Livermore DM, Williams RJ (1987) Expression of H1 outer-membrane protein of Pseudomonas aeruginosa in relation to sensitivity to EDTA and polymyxin B. *J Med Microbiol* 24: 267-274

Saint-Ruf C, Crussard S, Franceschi C, Orenga S, Ouattara J, Ramjeet M, Surre J, Matic I (2016) Antibiotic Susceptibility Testing of the Gram-Negative Bacteria Based on Flow Cytometry. *Front Microbiol* 7

Sakayori Y, Muramatsu M, Hanada S, Kamagata Y, Kawamoto S, Shima J (2003) Characterization of Enterococcus faecium mutants resistant to mundticin KS, a class IIa bacteriocin. *Microbiol-Sgm* 149: 2901-2908

Song MR, Liu Y, Huang XY, Ding SY, Wang Y, Shen JZ, Zhu K (2020) A broad-spectrum antibiotic adjuvant reverses multidrug-resistant Gram-negative pathogens. *Nat Microbiol* 5: 1040-+

Stan-Lotter H, Gupta M, Sanderson KE (1979) The influence of cations on the permeability of the outer membrane of Salmonella typhimurium and other gram-negative bacteria. *Can J Microbiol* 25: 475-485

Su YB, Kuang SF, Ye JZ, Tao JJ, Li H, Peng XX, Peng B (2021) Enhanced Biosynthesis of Fatty Acids Is Associated with the Acquisition of Ciprofloxacin Resistance in Edwardsiella tarda. *Msystems* 6

Unemoto T, Tsuruoka T, Hayashi M (1973) Role of Na + and K + in preventing lysis of a slightly halophilic Vibrio alginolyticus. *Can J Microbiol* 19: 563-571

Xie YT, Yang LH (2016) Calcium and Magnesium Ions Are Membrane-Active against Stationary-Phase Staphylococcus aureus with High Specificity. *Sci Rep-Uk* 6

Yan J, Bassler BL (2019) Surviving as a Community: Antibiotic Tolerance and Persistence in Bacterial Biofilms. *Cell Host Microbe* 26: 15-21

Yang J, Zeng ZH, Yang MJ, Cheng ZX, Peng XX, Li H (2018) NaCl promotes antibiotic resistance by reducing redox states in Vibrio alginolyticus. *Environ Microbiol* 20: 4022-4036

Yang MJ, Xu D, Yang DX, Li L, Peng XX, Chen ZG, Li H (2020) Malate enhances survival of zebrafish against Vibrio alginolyticus infection in the same manner as taurine. *Virulence* 11: 349-364

Yao Z, Guo Z, Wang Y, Li W, Fu Y, Lin Y, Lin W, Lin X (2019) Integrated Succinylome and Metabolome Profiling Reveals Crucial Role of S-Ribosylhomocysteine Lyase in Quorum Sensing and Metabolism of Aeromonas hydrophila. *Mol Cell Proteomics* 18: 200-215

Yazdankhah S, Rudi K, Bernhoft A (2014) Zinc and copper in animal feed - development of resistance and co-resistance to antimicrobial agents in bacteria of animal origin. *Microb Ecol Health Dis* 25

Zhang S, Wang J, Jiang M, Xu D, Peng B, Peng XX, Li H (2019) Reduced redox-dependent mechanism and glucose-mediated reversal in gentamicin-resistant Vibrio alginolyticus. *Environ Microbiol* 21: 4724-4739

Zhang S, Yang MJ, Peng B, Peng XX, Li H (2020) Reduced ROS-mediated antibiotic resistance and its reverting by glucose in Vibrio alginolyticus. *Environ Microbiol* 22: 4367-4380

Zhang Y, Gu AZ, Cen T, Li X, He M, Li D, Chen J (2018) Sub-inhibitory concentrations of heavy metals facilitate the horizontal transfer of plasmid-mediated antibiotic resistance genes in water environment. *Environ Pollut* 237: 74-82

Zhang YJ, Boyd SA, Teppen BJ, Tiedje JM, Li H (2014) Organic acids enhance bioavailability of tetracycline in water to Escherichia coli for uptake and expression of antibiotic resistance. *Water Res* 65: 98-106

Zhang YM, Rock CO (2008a) Membrane lipid homeostasis in bacteria. *Nat Rev Microbiol* 6: 222-233

Zhang YM, Rock CO (2008b) Thematic review series: Glycerolipids - Acyltransferases in bacterial glycerophospholipid synthesis. *J Lipid Res* 49: 1867-1874

Zhao XL, Chen ZG, Yang TC, Jiang M, Wang J, Cheng ZX, Yang MJ, Zhu JX, Zhang TT, Li H *et al* (2021) Glutamine promotes antibiotic uptake to kill multidrug-resistant uropathogenic bacteria. *Sci Transl Med* 13

Supplementary Materials for

Magnesium modulates phospholipid metabolism to promote bacterial phenotypic resistance to antibiotics

Hui Li[1,2,†], Jun Yang[1, 2, †], Su-fang Kuang[1] , Bo Peng[1,2, *]

*Corresponding author. Email: pengb26@mail.sysu.edu.cn

This PDF file includes:

Tables EV1 to EV3
Figures EV1 to EV6

Table EV1 Comparison in components in LBS and SWT

	LBS	**SWT**
Tryptone(%)	1	1
Yeast extract(%)	0.5	0.5
NaCl(mM)	171	210
$MgSO_4$(mM)	0	35
KCl(mM)	0	7
$CaCl_2$(mM)	0	7

Table EV2 Primes used in the present study

gene		KEGG entry	Sequences (5'-3')	gene		KEGG entry	Sequences (5'-3')
accA	Forward	N646_1411	AAAGGTCGTGAAACCAAAGA	*fadD*	Forward	N646_4025	CATTATTTACTGCGATCCTCG
	Reverse		AGCCGTGTCGATAAATGTG		Reverse		CCATATTGAGATATTTGTCTGGG
accB	Forward	N646_1967	TCAAGCACCAATTCACTACG	*fadE*	Forward	N646_1395	TATCCCAACTGATGTCAAAGG
	Reverse		ACTTTCTGACCCACTTCTACG		Reverse		CAACCGACAGACACTCAACC
accC	Forward	N646_1968	AGAAGTGACTGGTGCTGTGG	*fadB*	Forward	N646_2210	ATCACTAAAACGCCCAGAAAA
	Reverse		GGATAGTGTCTGCCTTTGGAC		Reverse		GCTGAAGCCGCCAAAGTA
accD	Forward	N646_1292	CGAACTTGAGCCACAGGATA	*fadA*	Forward	N646_1311	CAGATTAGCGGCCAGTTTCT
	Reverse		ACGACTGAACCCATTGAACC		Reverse		TCAAGCGGCGGTTAATGT
accD	Forward	N646_4704	AAGTTTGTCCGAGCAGTTGA	*fadA*	Forward	N646_2209	ATTGCGGGCTGCGATC
	Reverse		GAGACGCCACCATAAGTTTG		Reverse		GCACACGGCAGAGACTGC
fabD	Forward	N646_1131	CTCGCCTGGTCAAGTCGT	*fadH*	Forward	N646_1258	AAGTGCTGCCCTGCTCG
	Reverse		TGCTGGCTTCATAAGTGCA		Reverse		ATGATGGCGTCGAGTTAATG
fabH	Forward	N646_1132	GACCGTTCAACCATCATCCT	*fabR*	Forward	N646_2038	TTTGCTACTACGCCAACTGATGCGT
	Reverse		GCCATTTATCCGCATCTTG		Reverse		CGCTCACGCAACAACAAACGAA
fabH	Forward	N646_1439	GACGCTCCAACATGGCTAG	*fadR*	Forward	N646_1147	AATGCTAGGCGCTGGAA
	Reverse		AGTTCGCTGGTGACAATAAGA		Reverse		TGAATGCGGCTTCCTG
fabH	Forward	N646_4350	GGAAGACAACGGTTACTGGG	*arcA*	Forward	N646_1744	TGGGTTGAATGGTTTAGTGATG
	Reverse		TGCGGAATCACAACATCG		Reverse		TGAAGCCAGTGACGGTGAA
fabB	Forward	N646_1292	TTGACAGTGCGCCCATC	*crp*	Forward	N646_1004	AAGGTTGCTGCTACTTGCTGA
	Reverse		TGTCTTGCTACGCCATTTAAGA		Reverse		GCTTCGGATTGGTAATGGTT
fabB	Forward	N646_3036	CAACATTAATGCTGCGGCT	*crp*	Forward	N646_1885	CAAAACAACCAGACGCAATG
	Reverse		TGAGCGGCCCACATTAC		Reverse		CTCACGAGAACAGCCAACAAT

fabF	Forward	N646_1128	GGTGTTGCTATCGGCTCA	*gpsA*	Forward	N646_1922	GTGCGGGTATGTCTGATGG
	Reverse		ATGTTTACAATGGTCGAAGGA		Reverse		ATAAAGGTTTCTGGCTGTGC
fabF	Forward	N646_3033	AACTGCCAAAGCACTACAAGC	*plsB*	Forward	N646_2043	GCTTAGTTCGCTTTAGTCCC
	Reverse		TGATGAGCCGTATGCGATAC		Reverse		CACTTGGCGTTGTGGC
fabG	Forward	N646_1130	CAACCTAACGCCAATCTACC	*plsY*	Forward	N646_2566	CGCCAAGAATGATAGGGTC
	Reverse		CCACGAGACGCAACTTCA		Reverse		TTATTAGGTTCGGTTTCCAGT
fabG	Forward	N646_3034	GACCGAAGAAGAATGGGATG	*plsC*	Forward	N646_1749	CGATTCGCTCGGTCAA
	Reverse		TGCGCTGTAGTTAGTTTGACC		Reverse		TACTGTTTCTGCGGCTGT
fabG	Forward	N646_3826	AGTAAAGGCGGCGTCATC	*cdsA*	Forward	N646_1423	TTGCTGCCCTTGTGCC
	Reverse		TCTGGCAGGTTCTTGGTCA		Reverse		GCCAAGATTTCGTCGTTTT
fabG	Forward	N646_4505	CCCAAGGCGTTATCATCA	*pgsA*	Forward	N646_1026	GTTTTGGCGCGTTTATT
	Reverse		TTCGGGTTTCATTTGCTCT		Reverse		TTTCTCGCGCAATCATC
fabZ	Forward	N646_1416	GAGAAGTACCTTCACGCGAT	*pgpA*	Forward	N646_2838	ATGAGTTTGCGGGCTTT
	Reverse		CTGTTGCCTGAGCCATTG		Reverse		TCCCGCCACGATATCAT
fabV	Forward	N646_4267	AGTAATGGGCGGCGAAG	*pgpB*	Forward	N646_3562	TTTCTTTGGCGGGTTGT
	Reverse		TGGGTGCGTAATGTCAGG		Reverse		CTTCAGGGCGGTGCAT
fabV	Forward	N646_0267	GGTGGTTTACTCACTGGCATC	*pssA*	Forward	N646_2008	GATAAAACCGCCAACGA
	Reverse		TCTTCACCGCCCATTACC		Reverse		TTACGTGCGGCGATATT
tesA	Forward	N646_4268	AGCATTTCTGGCGATACAAC	*psd*	Forward	N646_1916	CACTCTGCGCCAAATG
	Reverse		GGAGGGAAACCTCTTAGGC		Reverse		ACGAGGCGGAGTGATC
tesB	Forward	N646_0021	CTTTGGATTCGTGCTAATGG	*pldA*	Forward	N646_4183	CTTTTTAGGTCGCCAGAAC
	Reverse		ATAGAGTGGTCAATGGTGGC		Reverse		CATAACCCGCTGAGTATTGT
yciA	Forward	N646_1052	TGTCTCAGCTCGACTTAGCG	*pldB*	Forward	N646_2069	GATCTCTACCGCCAAGGT
	Reverse		GGGTTTGACCCATACTTCCA		Reverse		AGTGCGCGATGATGAAG
fadL	Forward	N646_1315	CTAAGTATTGGCGCAACGTACG	*glpQ*	Forward	N646_1500	CTATCCAACCCGATTCCC
	Reverse		GCCGCCGACTTGTTCTG		Reverse		ACCAAGGCGCTTTAATTT

fadL	Forward	N646_1316	CTGCCTTCGCCGATGAT	*glpQ*	Forward	N646_3581	AAAAGTCCAATGCCGCA
	Reverse		GAAATTCGCGATTGGTTTG		Reverse		GTAACCGGCTTGTTGGAG
fadL	Forward	N646_3657	TTATCTGCGGGTGCCTCT	*glpQ*	Forward	N646_3723	CACAAATGGCGCTATCTG
	Reverse		GTCACGCCCGTCACCAT		Reverse		CCATCGGCTTCTTCACTC
fadD	Forward	N646_1045	TGTTCTTGAGCTGGTGGAAA	*glpQ*	Forward	N646_3724	GACTTGTGAAGCCCGC
	Reverse		AACACGCAATGACGAGGTAT		Reverse		AGATACTCAGGGCCAATAAAC
fadD	Forward	N646_2540	GCATCGGTCGATTCTTCC	*etuC*	Forward	N646_3725	CTTTTAAGCGCTGATGATGA
	Reverse		CGCCAATCTTAACCTGTGC		Reverse		GTTAGACCGGGTCTCTCTC
fadD	Forward	N646_3023	CTCTGATGATGCCAAACCTAC	*adhE*	Forward	N646_1240	AGCGATGCTGCACGAA
	Reverse		ACGAGGAGTGTAAAGTGGGTT		Reverse		CCTGTAACTAATATGGCTGAAC

Table EV3 Primers used in the present study for construction of gene-deleted mutants

gene		primer (5'-3')
fadR	P1	aaaaaggatcgatcct TACTTCCCCTGAACTCAAGCAC
	P2	TGTCAGCGCTTATCTACTTTTTATCCAATATTGATTTCTG
	P3	ATAAAAAGTAGATAAGCGCTGACAAGTTGGATAAAC
	P4	atcgcatgcggtacc GCAAAGAGATGACTTGCATAATGAGTA
	P5	ATGGTCATAAAGGCGAAAAGCC
	P6	TTAGCTGTCGTCTTCCGTGAAGTT
	P7	AATAGTGCTTAAGTATCTGTTTGT
	P8	ATGACCATAGTGTTGCAAGA
arcA	P1	aaaaaggatcgatcct GACCTCAAGTTACTGTATGGGTTCC
	P2	TAGCGGTTAAATTGGCGGTACCTAAATTTGTGACA
	P3	TAGGTACCGCCATAGATTTAACCGCTAATATGCAAAGGG
	P4	atcgcatgcggtacc ATTGATGGCAGGCTGTAGTTCC
	P5	ATGCAAACCCCGCAGATTCT
	P6	TGGCGATGATTTCTGGCGT
	P7	CGACGGCAAAGCTTTCCTC
	P8	AAAAGTTGGTTGGAACAAAGGAA
plsB	P1	aaaaaggatcgatcct TTAGGTGTTCCTCTGCGGCAT
	P2	AAGGTAAAACGGAAAGTTCACAGCCTCAATAGGTATTC
	P3	GCTGTGAACTTTTAACCGTTTTACCTTCTTCCAATAAGA
	P4	atcgcatgcggtacc AGCTATTTTTAGGCTTGGCTTTTA
	P5	ACAACGATAATGATGTCCCAACC
	P6	GAACGACCACCCTCACTGAAGTA
	P7	GCTCATCATTGGCTGCGTCT
	P8	TGCTGACCATGAACCCGC
waaf	P1	aaaaaggatcgatcct AGTTGTGGGTTCGCTGTGTTGA
	P2	GAACTAACATGAGCTTTGTTTTTCCAGTATAGGAATT
	P3	GAAAAACAAAGCTCATGTTAGTTCGTATTGTTTATACCTT
	P4	atcgcatgcggtacc TTGGCGTAGTTCTGACACGATT
	P5	AACGCCATCCAGATAGCCAAAT
	P6	AGGTTTCAAGCCCGCCAAGA
	P7	ATATGTGGGTACTACAGTTGCTGCA
	P8	CATCTAATACCTGTTCGTCCTC
lpxA	P1	aaaaaggatcgatcct TACGACCTGTTGCCACGTTTG
	P2	ATTCGCCAATTAATTAAAACTCTCGACGAGCACAC
	P3	GAGAGTTTTAATTAATTGGCGAATGAACCAATAAATAA
	P4	atcgcatgcggtacc ATTTTAAAGATGCGCTTCTGACG
	P5	GGCAGCGGTGGTAGAAGAGG
	P6	AACGGGTGAATCGCAGACAG
	P7	ATTGATGAGATGAATAAGCGCCT
	P8	TAACTCGCTACCACGACTGCCT
lpxC	P1	aaaaaggatcgatcct AGACGGTTGGTAATACAGTGAAG

	P2	GCCAAGTATTTACTGCTTGCCTCTCAAAAATTTGC
	P3	AGAGGCAAGCAGTAAATACTTGGCATTAGAATTAATAA
	P4	atcgcatgcggtacc CTGGAGAAATCTTACAGCTTAAC
	P5	ATTGAATCAGACGAGCAACG
	P6	CGAATGTAGTCCACTCCCAC
	P7	AGAATGCCGTTCAAGGTATTGC
	P8	TTTACTTAAAGTGGTGACTGATT
pgpA	P1	aaaaaggatcgatcct AAGCACTAGAGCGAGCTCATTAC
	P2	GTTCATGGTTTAATCCTTAAACCTATACTGCTAGTTT
	P3	AGGTTTAAGGATTAAACCATGAACTAAACACTGGACGT
	P4	atcgcatgcggtacc ATACCCTCGTGGTAGCGGCAT
	P5	GGCACAATTACCATTTACGG
	P6	TAGAAACAGGGCAACACCAG
	P7	CATTTTTCGAACTGGCTGATT
	P8	GCAACGTGGTTATGACCAATT

Small letters are homologous recombination sequences with pDS132 plasmid.

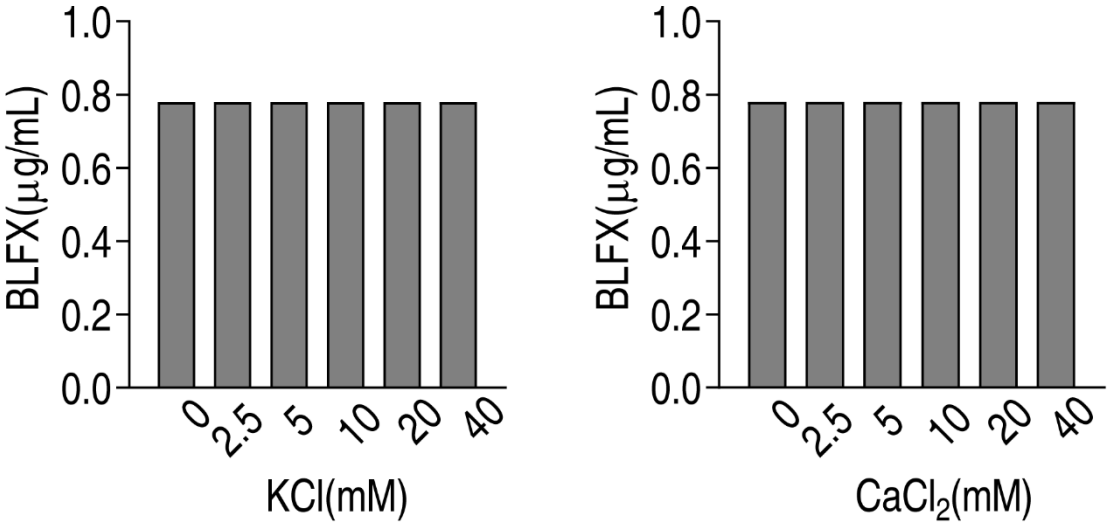

Figure EV1 MIC of ATCC33787 to BLFX in the absence or presence of the indicated concentrations of KCl or $CaCl_2$.

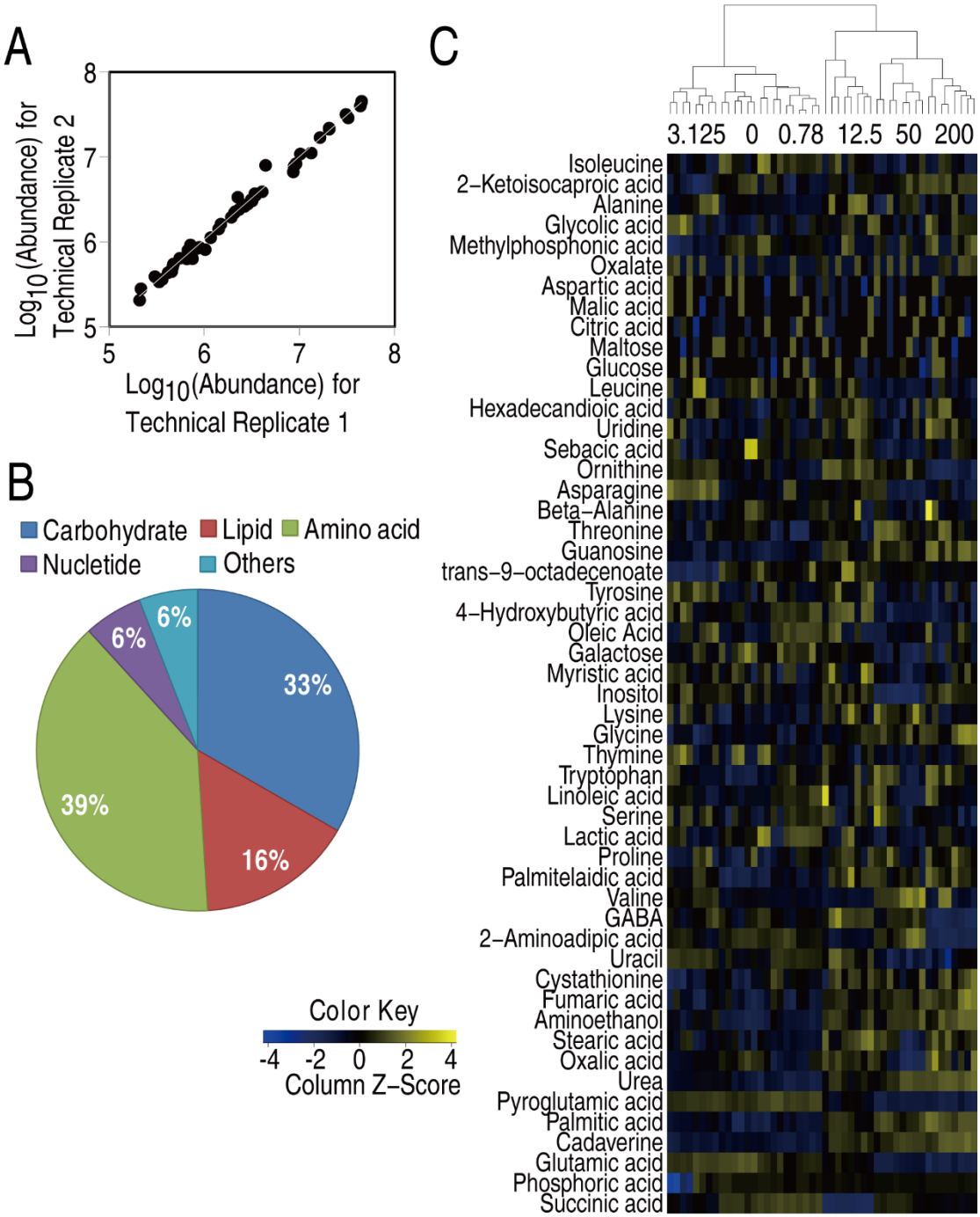

Fig EV2 Metabolic profiles of *V. alginolyticus* in different concentrations of $MgCl_2$.

A. Reproducibility

B. Percentage of metabolites in every category

C. Heatmap of metabolites

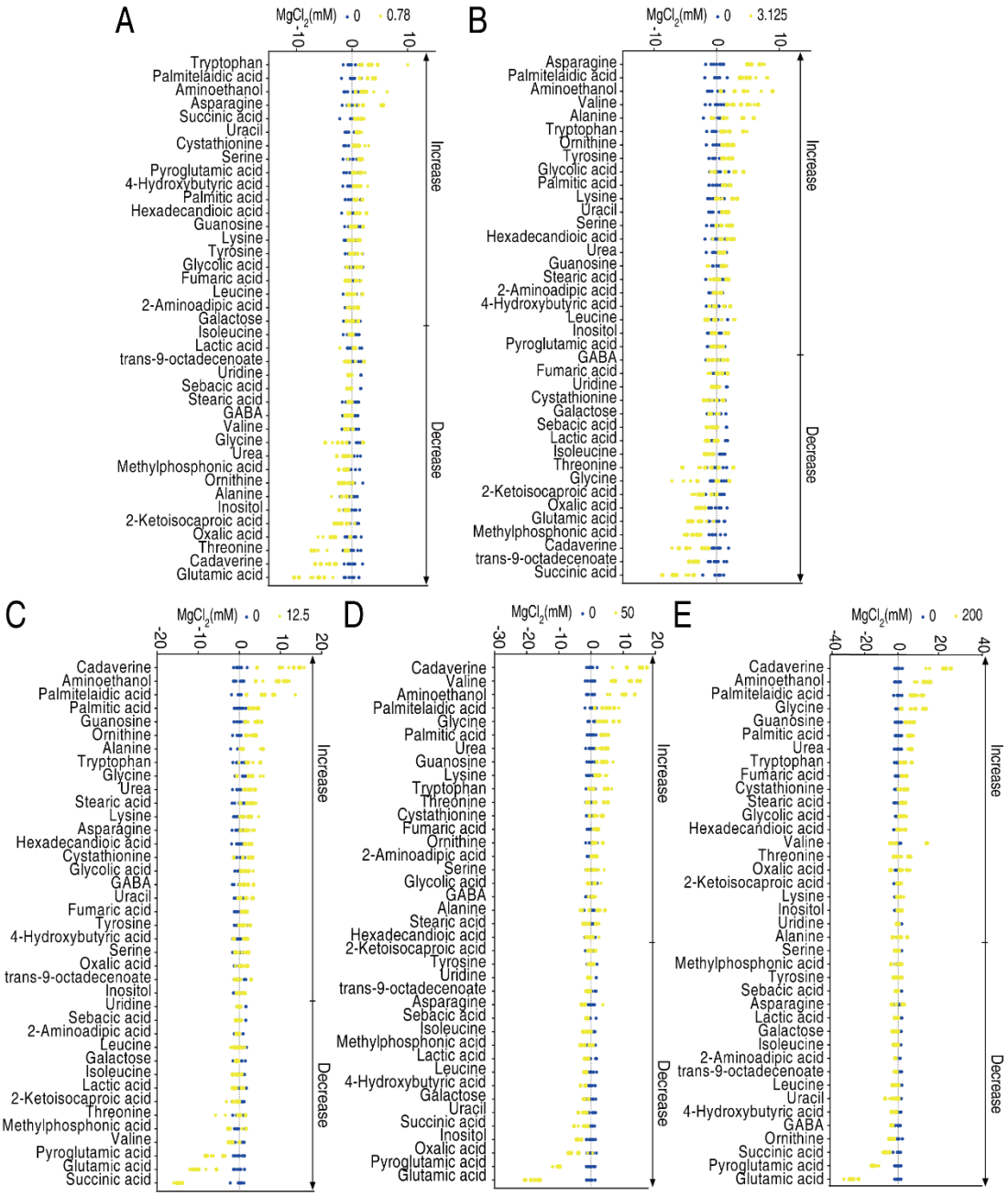

Fig EV3 Heatmap and Z score plots of differential metabolites.

A. Heatmap of differential metabolites

B-F. Z score plots of differential metabolites.

A

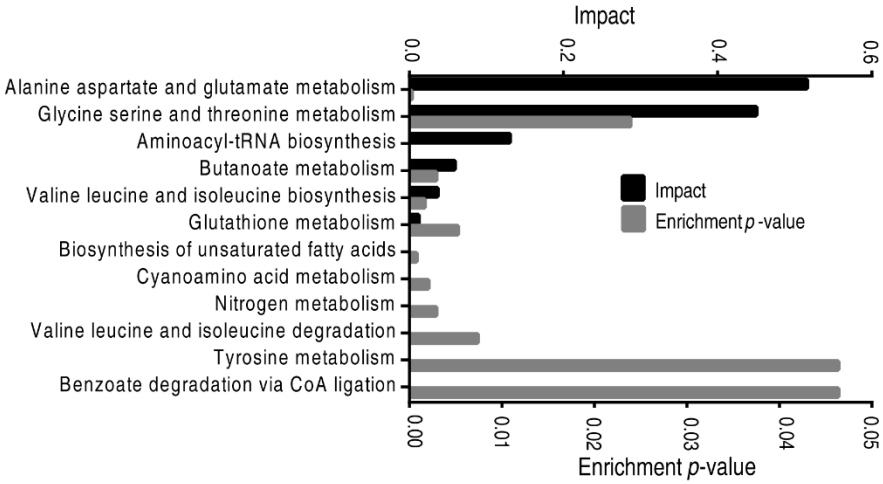

B

$MgCl_2$(mM)	0	0.78	3.125	12.5	50	200
1. Alanine, aspartate and glutamate metabolism						
Alanine	1898969	1669909	2270982	2429767	1942138	1899416
Succinic acid	50409684	51838313	44608730	35763780	48097737	45062382
Glutamic acid	46612570	41399307	44320733	39223184	32681397	30791721
Asparagine	519714	561512	649662	561568	500971	504444
Fumaric acid	6346076	6425403	6308485	7248083	7407043	8116023
2. Glycine, serine and threonine metabolism						
Threonine	907651	930072	1057811	1012039	887065	876568
Glycine	628747	595891	554133	717008	804935	876577
Serine	3249673	4071405	4213032	3786036	4004807	3071669
Tryptophan	553553	703724	643187	666468	666188	725451
3. Aminoacyl-tRNA biosynthesis						
Alanine	1898969	1669909	2270982	2429767	1942138	1899416
Glutamic acid	46612570	41399307	44320733	39223184	32681397	30791721
Valine	4592928	4354830	5990598	3998236	7983101	5108404
Leucine	276023	278630	279692	258314	228627	240021
Isoleucine	1804803	1766736	1530961	1661897	1503637	1550118
Threonine	907651	930072	1057811	1012039	887065	876568
Glycine	628747	595891	554133	717008	804935	876577
Asparagine	519714	561512	649662	561568	500971	504444
Lysine	593086	626792	801008	872538	965546	687658
Serine	3249673	4071405	4213032	3786036	4004807	3071669
Tyrosine	907651	930072	1057811	1012039	887065	876568
4. Butanoate metabolism						
Glutamic acid	46612570	41399307	44320733	39223184	32681397	30791721
GABA	5005243	4686142	4996330	6093403	5256494	3043750
Succinic acid	50409684	51838313	44608730	35763780	48097737	45062382
Fumaric acid	6346076	6425403	6308485	7248083	7407043	8116023
5. Valine, leucine and isoleucine biosynthesis						
Valine	4592928	4354830	5990598	3998236	7983101	5108404
Leucine	276023	278630	279692	258314	228627	240021
Isoleucine	1804803	1766736	1530961	1661897	1503637	1550118
Threonine	907651	930072	1057811	1012039	887065	876568

$MgCl_2$(mM)	0	0.78	3.125	12.5	50	200
6. Glutathione metabolism						
Glutamic acid	46612570	41399307	44320733	39223184	32681397	30791721
Glycine	628747	595891	554133	717008	804935	876577
Ornithine	496661	448553	570268	618310	548551	380285
Cadaverine	21689312	19397099	19801296	27806135	28645266	31463303
7. Biosynthesis of unsaturated fatty acids						
Palmitic acid	18685587	19545136	20263877	22225172	23175886	24379308
Stearic acid	11791565	11504866	11958456	13301491	11916753	13119749
8. Cyanoamino acid metabolism						
Glycine	628747	595891	554133	717008	804935	876577
Asparagine	519714	561512	649662	561568	500971	504444
Serine	3249673	4071405	4213032	3786036	4004807	3071669
9. Nitrogen metabolism						
Glutamic acid	46612570	41399307	44320733	39223184	32681397	30791721
Glycine	628747	595891	554133	717008	804935	876577
Asparagine	519714	561512	649662	561568	500971	504444
Tryptophan	553553	703724	643187	666468	666188	725451
10. Valine, leucine and isoleucine degradation						
Valine	4592928	4354830	5990598	3998236	7983101	5108404
Leucine	276023	278630	279692	258314	228627	240021
Isoleucine	1804803	1766736	1530961	1661897	1503637	1550118
11. Tyrosine metabolism						
Succinic acid	50409684	51838313	44608730	35763780	48097737	45062382
Tyrosine	907651	930072	1057811	1012039	887065	876568
12. Benzoate degradation via CoA ligation						
Succinic acid	50409684	51838313	44608730	35763780	48097737	45062382
Fumaric acid	6346076	6425403	6308485	7248083	7407043	8116023

Fig EV4 Pathway enrichment of differential metabolites.

A. Pathway enrichment of differential metabolites

B. Differential metabolites in enriched pathways

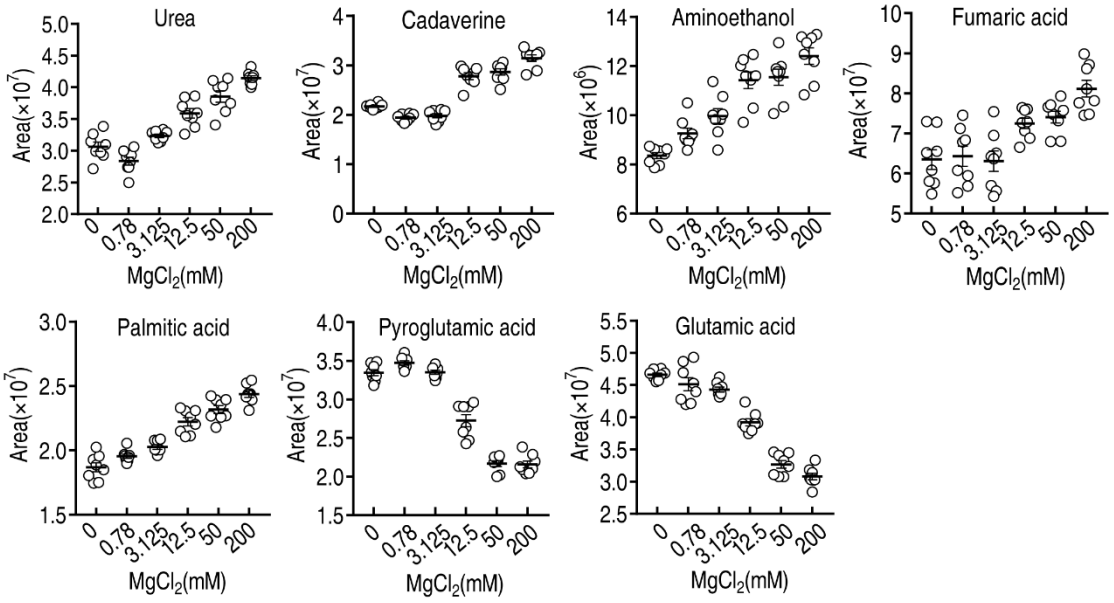

Fig EV5 Scatter plots of differential metabolites identified by S-plot.

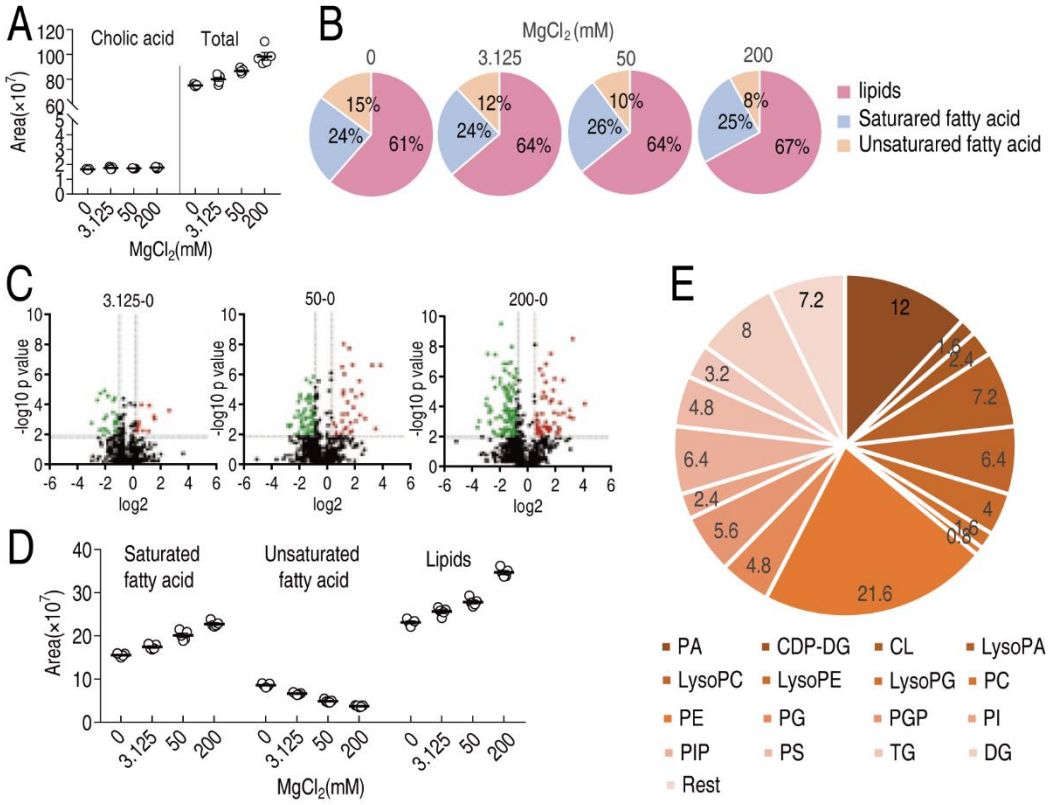

Fig EV6 Lipidomes in the different concentrations of $MgCl_2$.

A. Area of fatty acids in the presence of indicated concentrations of $MgCl_2$.

B. Percentage of lipids, saturated fatty acid and unsaturated fatty acid in the presence of indicated concentration of $MgCl_2$.

C. Volcano plots of lipidomics of indicated concentration of $MgCl_2$ as compared to non-treated control.

D. Relative abundance of saturated fatty acids, unsaturated fatty acids and lipids in the presence of indicated concentrations of $MgCl_2$.

E. Relative percentage of indicated lipids.